

Three Events of Strong Deep Moist Convection in The Netherlands

Pieter Groenemeijer

*“All thunderstorms are dangerous,
but some thunderstorms are more dangerous than others.”*

Contents

1	Introduction	5
1.0.1	European severe storm research	5
2	Deep Moist Convection	7
2.1	An ingredients-based forecast methodology	7
2.2	Parcel theory	7
2.2.1	Limitations of parcel theory	11
3	Organized Deep Moist Convection	13
3.1	Single cells	13
3.1.1	Dynamics	13
3.2	Multicell storms and squall-lines	14
3.2.1	Dynamics	14
3.2.2	Multicell cluster storms	16
3.2.3	Multicell line storms or squall-lines	17
3.3	Supercells	21
3.3.1	Dynamics	21
3.3.2	Radar characteristics of supercells	23
4	Doppler Radar	27
4.1	Principles of a radar	27
4.2	Principles of a Doppler-radar	27
4.2.1	Dual-PRF and unfolding	28
4.2.2	De-aliasing	29
4.2.3	Detection of mesocyclones	30
5	Cases	33
5.1	A squall line in winter, January 28 2003	33
5.1.1	Event description	33
5.1.2	Synopsis	33
5.1.3	Radar data	38
5.1.4	Case discussion	47
5.2	30th of July 2002, Multicell thunderstorms with strong outflows	49
5.2.1	Event description	49
5.2.2	Synopsis	49
5.2.3	Radar data	49
5.2.4	Case discussion	56
5.3	Embedded HP-mini-supercell, 2nd of May 2003	58

5.3.1	Event description	58
5.3.2	Synopsis	58
5.3.3	Radar data	59
6	Conclusions and recommendations	69
6.1	Radar	69
6.2	Convective forecasting	70
6.2.1	Recommendations for enhancement severe (convective) storm forecasting at the KNMI	71

Preface

The inspiration to do the research that has resulted in this report started to arise in Norman, Oklahoma. Six co-students and I went there to learn about deep moist convection at the School of Meteorology of the University of Oklahoma. There, I have learned a lot about the topic from people like Howard Bluestein and Joshua Wurman. A visit to the Storm Prediction Center – also in Norman – and participating in the European Conference on Severe Storms in Prague, Czech Republic, in the summer of 2002, made me get more and more interested in the problem of forecasting of severe thunderstorms. I was curious what could be done in this topic in my home country the Netherlands. It turned out to be the right idea at the right time, since Iwan Holleman at the KNMI had a dataset from the KNMI radar that was waiting for meteorological analysis. The dataset included both reflectivity data and Doppler-data obtained with the institutes radar of which the settings had been optimized for Doppler-analysis one and a half year earlier. I like to thank Iwan Holleman, the KNMI’s “radar-man”, who was enthusiastic about the idea of me looking deeper into the data. He arranged a workplace for me at the KNMI and helped me with many practical problems I encountered. His algorithm for removing de-aliasing errors and the solid software that he had developed enabled me to visualize radar data without much effort, which resulted in the colorful pictures found in this report.

If found that many meteorologists at the KNMI are interested in the topic of severe thunderstorms. I had many interesting discussions from which this report has greatly benefited. In particular I talked a lot with Oscar van der Velde...maybe a bit too much.... I also had discussions with Adrie Huiskamp, Han Mellink, Menno van der Haven, Robert Mureau and others. It was a pleasure to have my friends from the Tornado Team Utrecht and my colleagues of ESTOFEX to be interested in my research and telling them about it. I would also like to thank Aarnout van Delden of the Institute for Marine and Atmospheric Research Utrecht (IMAU) at Utrecht University, who supported me to do this research as a part of my education at the University. Iwan Holleman, Aarnout van Delden and Menno van der Haven have read the first version of this report and did many suggestions for improvement for which I want to thank them. Finally, I thank Nander Wever who has programmed an application for plotting surface observations on a map of The Netherlands which I could use well in this study.

Chapter 1

Introduction

There are numerous reports of severe weather occurring in The Netherlands every year, some of which are related to thunderstorms. The Netherlands however, storm force winds associated with extratropical low-pressure systems are a greater weather hazard than summertime thunderstorms. Nevertheless thunderstorms are also potentially dangerous. They bring lightning, and may be accompanied by very strong wind gusts, large hail, and occasionally tornadoes. Another potential hazard is flash flooding. In recent years a few very intense events have occurred that have drawn the attention of meteorologists. On June 7th 1997 a strong bow-echo struck the western Netherlands that caused a small number of fatalities (Groenland, 2002). On June 6th 1998 very large hail – up to more than 8 cm in diameter – did considerable damage in central and western parts of the Netherlands (Kuiper and De Hond, 1999). In an average year numerous reports of flash flooding, severe wind gusts, large hail and (mostly weak) tornadoes reach the Royal Netherlands Meteorological Institute KNMI and this type of severe weather is by no means limited to The Netherlands. A few extreme severe weather events from neighboring countries include a strong tornado that hit Tournai, Belgium on August 14th, 1999, which was declared to be a national disaster (RMI, 2000). Other events include a severe squall-line in Strasbourg (16 dead, 6 July 2001; DPA/AFP) and a squall line/derecho that hit Berlin and surroundings on 10 July 2002 (8 dead; Gatzen, 2003). It is often thought that severe convective events occur most often in summer, primarily because the atmosphere is then on average the most unstable. However, they also occur in winter, when instability is generally less but strong dynamic forcing and strong wind shear seem to be responsible. One such event is studied in depth herein.

1.0.1 European severe storm research

Severe storm research in Europe is still in its early stages. However, the increasing number of publications in scientific literature on severe thunderstorms in Europe gives the impression that there is a growing attention for the subject. Currently, a large problem is the availability of severe weather events, especially because events of hail, tornadoes and severe wind gusts occur on a spatial scale that is much too small to be resolved by operational synoptic observation networks. Data are present in archives of insurance companies, media archives and

volunteers, but it is not well accessible for scientific research. Some volunteers have organized into nationally operating networks, (Dotzek, 2002; TORRO¹) or gather data in the context of a volunteer organisation of meteorology enthusiasts (VWK²). Some of these datasets have formed the basis of articles in scientific journals (Dotzek, 2001). In this study we have used some data gathered by volunteers, but others have already managed to do entire climatological studies on European severe storm events. For example, tornado climatologies have been published concerning France (Dessens and Snow 1989), Germany (Dotzek, 2001), Austria (Holzer, 2001), The United Kingdom (TORRO) and Europe as a whole (Dotzek, 2003). Moreover, two conferences on the topic of severe storms have been organised (Eurotornado 2000; ECSS, 2002). In order to solve the problem of data availability, plans are being developed for the establishment of a European Severe Storms Laboratory (Dotzek, 2002). Within the KNMI there are also plans to study severe weather events more systematically (Mellink, pers. comm.). All this illustrates that this part of the meteorological science is rapidly developing, which is not surprising as the demand of society to be protected from the weather keeps increasing.

¹The Tornado and Storm Research Organisation, Oxford, UK

²Vereniging voor Weerkunde en Klimatologie, The Netherlands

Chapter 2

Deep Moist Convection

The subject of this study is the occurrence of severe weather in association with *deep, moist convection* (DMC). By DMC we mean the convective overturning of the entire troposphere or a large part thereof, which automatically implies that condensation of water (i.e. moist processes) will occur. We use the term DMC (Doswell, 2001) instead of the more common term “thunderstorm”, so that non-thundering convection is included.

2.1 An ingredients-based forecast methodology

DMC occurs in specific meteorological environments. That is, some specific boundary conditions must be met. Assessing if this is the case can be called an *ingredients-based forecast methodology* (Doswell, 2001). Environments in which DMC can develop are characterized by the presence of

- latent instability¹
- lift

Latent instability is a situation in which a parcel of air originating from some low atmospheric level will become warmer than its environment if it were lifted upward far enough. When this occurs, the parcel will become positively buoyant and will automatically accelerate upward. Latent instability is not necessarily a true instability, but a situation in which a forcing of finite magnitude may be needed to create a *real instability*, which is a flow perturbation that grows by positive feedback on itself. A short treatment of parcel theory follows, which we can use to find out if there is latent instability and if the instability can be released.

2.2 Parcel theory

In order to assess whether latent instability is present, one should evaluate if a parcel of air at some height in the troposphere can become positively buoyant

¹Slantwise convection can be driven by symmetric instabilities instead of latent instability, but slantwise convection is not thought to cause severe weather. For a more extensive discussion of instabilities such as latent instability, potential instability, conditional instability and symmetric instabilities see Schultz et al. (2000)

when it is lifted. Buoyancy is a quantity that arises in the vertical momentum equation. If we write this equation in terms of perturbations on a hydrostatically balanced base state, we obtain

$$\frac{dw}{dt} = -\frac{1}{\rho} \frac{\partial p'}{\partial z} - \frac{\rho'}{\rho} g. \quad (2.1)$$

We call the first term on the R.H.S. the pressure perturbation term and the second term is known as buoyancy. In an ideal gas, at speeds much smaller than the speed of sound, a parcel's buoyancy is dependent on its (virtual) temperature perturbation only, that is

$$B \simeq g \left(\frac{T'_v}{\bar{T}_v} \right), \quad (2.2)$$

where T'_v is the virtual temperature difference between the parcel and its environment, \bar{T}_v is the average virtual temperature (we assume $T'_v \ll \bar{T}_v$). Virtual temperature is almost equal to temperature except for a small term that incorporates the effects of water vapor content on the density of the air. From this point on, we will use T instead of T_v for simplicity. Thus, we can evaluate a parcel's buoyancy when we know the virtual temperature difference between the parcel and its environment as will be explained.

Making the assumption that no exchange of heat will take place between the parcel and its environment, its potential temperature θ is conserved if no condensation or evaporation of water takes place within it. If water vapor condenses to liquid water the equivalent potential temperature θ_e (and by approximation θ_{ep} and θ_w) are conserved quantities.² Using a thermodynamic diagram with lines of equal θ and θ_e/θ_w , it can be graphically evaluated whether latent instability is present using data obtained from a radiosonde sounding or a numerical weather model.

Fig. 2.1 is a so-called skew- T log p diagram showing a temperature and humidity profile that may be preceding the development of DMC. In fig. 2.1 an ascent curve is constructed for a parcel having the average properties of the air in the lowest 75 hPa. The parcel follows a dry adiabat along which θ is conserved up to the lifted condensation level (LCL) where condensation commences. Above the LCL θ_e and θ_w are conserved and the parcel will cool less with height due to the release of latent heat of condensation.

Making use of this, one can calculate the difference between the parcel's temperature and that of its environment if the parcel were lifted.

The level at which the parcel becomes positively buoyant is known as the *level of free convection* (LFC). Above the LFC, it will accelerate upward until it ultimately gets cooler than its environment. The level at which this occurs is known as the *equilibrium level* (EL) or *level of no buoyancy* (LNB).

The *convective available potential energy* (CAPE) is a measure for the amount of latent instability. If we assume that buoyancy is the only (volume) force working on the parcel, we obtain the following momentum equation,

²When one assumes that liquid water will fall out of a lifted parcel as condensation takes places, its pseudo-equivalent potential temperature θ_{ep} and wet-bulb potential temperature θ_w are conserved instead of the equivalent potential temperature θ_e . Since the actual difference between θ_e and θ_{ep} is very small, we will use them here interchangeably.

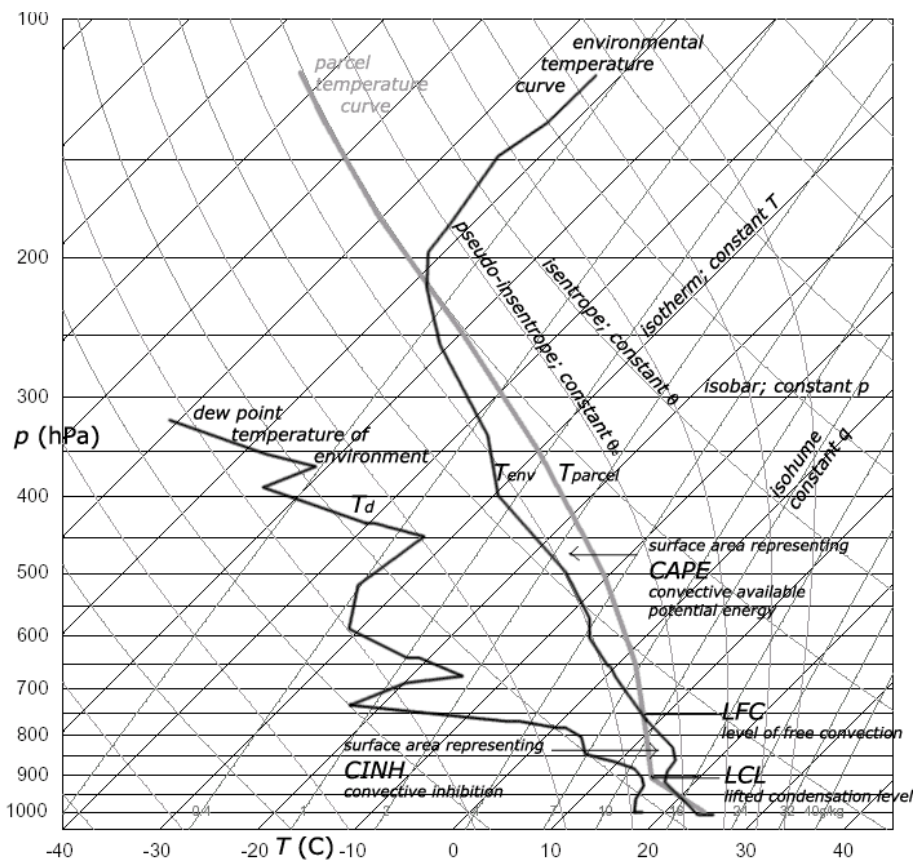


Figure 2.1: Skew-T log p thermodynamic diagram on which temperature and humidity data are plotted typical of a situation prior to the development of DMC.

$$\frac{dw}{dt} = B. \quad (2.3)$$

If we, for simplicity, allow for vertical velocities only and assume a stationary state (i.e. we have a full-grown constant updraft), we may integrate this equation from the LFC to the EL. This will give us the work the buoyancy force does or, equivalently, the amount of CAPE that is released,

$$CAPE = \int_{LFC}^{EL} B dz = \int_{LFC}^{EL} g \frac{T'}{T} dz. \quad (2.4)$$

In a skew- T log p diagram the amount of CAPE is proportional to the area between the parcel ascent curve and the environmental temperature curve.

An estimate of the updraft speed can be made by assuming all convective available potential energy is converted into kinetic energy of the air parcel. Using that $E_{kin} = \frac{1}{2}mw^2$ and assuming that the parcel has zero kinetic energy at the LFC, we obtain

$$w_{EL} = \sqrt{2 CAPE}. \quad (2.5)$$

CAPE will not be released until a parcel reaches its LFC. For this to occur, the rising parcel often has to overcome an amount of negative energy. This energy is called *convective inhibition* (CINH) and is represented by the area between curves just below the LFC. For parcels to be able to reach their LFC, CINH normally has to become small, so that air-parcels can get through this layer where they are negatively buoyant. This may happen through a number of processes such as

- lifting of air in the entire profile, which will act to destabilize the profile in case of potential instability. Warm layers inhibiting free DMC are cooled in this process.
- moistening or diabatic heating of the layer from which the potentially buoyant parcel originates
- differential temperature advection; that is, more cold advection or less warm advection aloft than below.

Once convection has initiated and a mature storm cloud forms, convective downdrafts will form in addition to the updrafts already present. Parcel theory can be used to help estimate what vertical speeds can be reached in these downdrafts. A frequently used method is to consider a parcel of unsaturated air in the environment of the updraft that becomes entrained into a storm cloud at mid-levels (e.g. 600 hPa). Upon entraining into the storm-cloud, it is assumed that this parcel will become saturated by evaporation of cloud droplets, rain or ice into it. This will result in cooling of the parcel. This cooling may be particularly strong if the entraining air was dry originally, so that a lot of evaporation takes place, before the parcel gets saturated. Because of this cooling, the parcel becomes negatively buoyant and accelerates downward. If the assumption is made that the parcel will stay almost saturated because of continuous evaporation of cloud droplets or precipitation, it will follow a moist adiabat. Since

the air surrounding it will have a steeper lapse rate the parcel becomes increasingly negatively buoyant. Its vertical velocity can be calculated by developing a quantity similarly to CAPE, downdraft CAPE, also known as DCAPE, DAPE or NAPE,

$$DCAPE = \int_{LFS}^{SFC} -B dz = \int_{LFS}^{SFC} -g \frac{T'}{\bar{T}} dz, \quad (2.6)$$

where LFS is the level of free sink and SFC denotes the earth's surface. The maximum downdraft velocity is then given by

$$w_{SFC} = \sqrt{2 DCAPE}. \quad (2.7)$$

The theory can be modified in such a way that the downdraft is allowed to become substantially sub-saturated under a certain level, after which it follows a dry adiabat to the surface, or –more realistically– will have a lapse rate somewhere between the moist and dry adiabats. In practice the level at which this occurs and the lapse rate to choose below it cannot be determined since they are highly dependent on the unknown size, form and numbers of the precipitation particles within the downdraft. Besides that, there are a number of more fundamental imperfections to parcel theory in general.

2.2.1 Limitations of parcel theory

Above, the concept of an air parcel was introduced. However, some unrealistic assumptions are made in parcel theory.

- Entrainment of environmental air into the parcel, which usually implies heat exchange between the parcel and its environment, is not accounted for.

This is certainly not realistic, for there is always entrainment of environmental air through the boundaries of a parcel, which usually implies an exchange of heat³.

- Radiational heat exchange is ignored
- The forces that arise due to pressure perturbations are neglected

In order to calculate CAPE we have neglected the respective terms in the vertical momentum equation. A more complete momentum equation is

$$\frac{dw}{dt} = -\frac{1}{\rho} \frac{\partial p'_d}{\partial z} + \left(\frac{-1}{\rho} \frac{\partial p'_b}{\partial z} + B \right), \quad (2.8)$$

Two terms of pressure perturbations are present in this equation. Following Doswell and Markowski (2001) we have made a distinction between dynamic and buoyancy-induced pressure perturbations. Dynamic pressure perturbations p'_d arise in fluids that are in motion, while buoyancy-induced pressure perturbations p'_b occur near every buoyant parcel even if it is at rest (see fig. 2.2).

³It can be shown using similarity theory that entrainment of environmental air must naturally occur in both thermals and thermal plumes. See for details e.g. Emanuel, 1994, chapter 2.

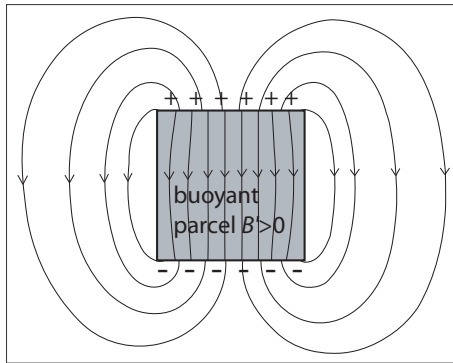


Figure 2.2: Buoyancy induced pressure perturbation p'_b near a positively buoyant parcel. Lines represent the vector field of the pressure gradient force. Based on a figure from Houze (1993).

We will see that p'_d is important when we consider the effects of convection in sheared flows. In an isolated updraft in a calm environment the dynamic pressure gradient will counteract the upward buoyancy force working on a parcel. However, in supercell convection it can be directed upward as well and add to the updrafts' strength. The buoyancy-induced pressure gradient p'_b plays an important role in the dynamics of squall-lines and offers an explanation for the so-called rear inflow jet.

Finally, an important disadvantage of parcel theory is that

- The weight of liquid and solid water, that will form in a real storm, is not accounted for.

All this is reason not to use the magnitude of latent instability only to assess the maximum updraft speed in a storm. Though a velocity can certainly be calculated from a CAPE value by the relationship $w_{max} = \sqrt{2 CAPE}$, it generally is not an accurate way to predict vertical motion in storms (Doswell and Rasmussen, 1994).

Chapter 3

Organized Deep Moist Convection

Deep moist convection can be seemingly randomly organized or exhibit particular structures. The various organized forms of DMC are known as *convective modes*, each having different dynamics. Each convective mode has its characteristic meteorological setting, characterized by a specific combination of latent instability, vertical wind shear and lift. Over the last decades an entire taxonomy of convective modes has been established. These convective modes include single cells, multicells (among which are quasi-linear convective systems) and supercells.

The most important factor to DMC organisation is wind shear. Generally, with increasing wind shear the convection will be more organized and self-sustaining. With equal amounts of CAPE, the threat of severe weather increases as wind shear gets larger (Craven et al., 2002). Fig. 3.1 shows the characteristic modes of convection to be expected as a function of wind shear magnitude and instability. It is important to recognize that apart from the magnitude of the wind shear and CAPE, factors like the change of *wind direction* with height and the amount of large-scale forcing for upward motion (lift) are also important. Furthermore, convection often changes from one mode to another during its lifetime even without change of the aforementioned environmental factors.

3.1 Single cells

Single cells or *ordinary cells* have relatively short lifetimes and their dynamics are quite simple. Fig. 3.2 shows the life cycle of an ordinary cell. They occur in an environment of low vertical wind shear.

3.1.1 Dynamics

In its initial stage a convective bubble forms as a quantity of air has reached its LFC. It accelerates upward up to the tropopause where it meets its equilibrium level. Gradually precipitation forms within the cloud, which negatively impacts the air's buoyancy. When the precipitation falls down, its evaporation cools the unsaturated sub-cloud layer, which further reduces buoyancy. In this way

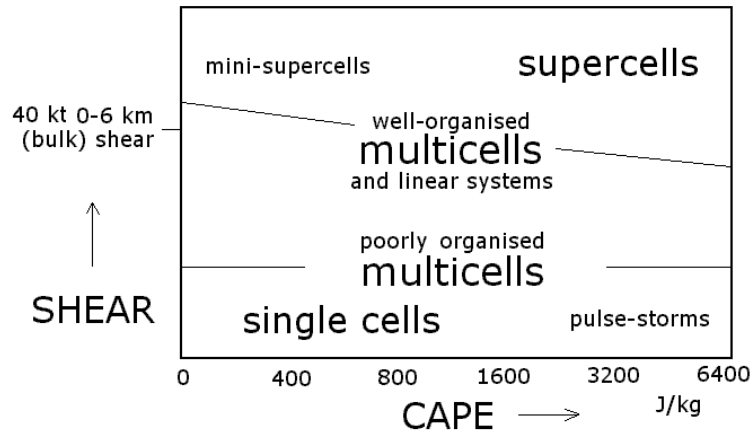


Figure 3.1: Convective modes to be expected given amount of wind shear and CAPE. 0-6 km bulk shear is the magnitude of the vector difference between the horizontal wind at 10 m and at 6 kilometers altitude.

a mass of cold air, frequently referred to as a cold pool, forms beneath the convective updraft.

As the cold pool spreads out over the earth's surface it cuts off the inflow of warm air flowing into the updraft. The remaining precipitation falls out and smaller water droplets and ice particles evaporate. This life cycle takes typically 30 to 50 minutes. Single cells are often the building blocks of larger convective systems. Single cells rarely produce severe weather. When they do, it is often in environments of extreme latent instability. These storms have very high tops and are sometimes called *pulse storms* (fig. 3.2).

3.2 Multicell storms and squall-lines

3.2.1 Dynamics

A multicell storm is a storm consisting of multiple convective updrafts and downdrafts. The key to the genesis of a multicell storm is the development of new convective cells along the boundary of the cold pool originating from an older cell. Such a boundary is often called an *outflow boundary* or *gust front*.

This is most likely to happen on the downshear side of the convective complex (i.e. the direction from which the low-level wind blows in a storm-relative reference frame). It is caused by rising motions that result from interaction of the cold pool-boundary and the environmental – potentially buoyant – air. During this ascent new air parcels reach their level of free convection and develop into a new convective cell.

Cell regeneration: RKW-Theory

Rotunno et al. (1988; hereafter RKW) found that vertical wind profiles with wind shear in the lowest kilometers and no or less shear aloft seem to be the

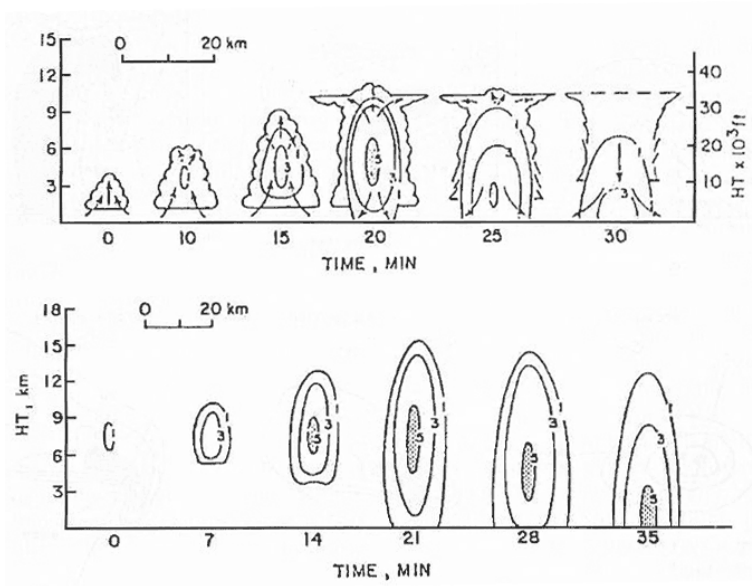


Figure 3.2: Life cycle of a single cell storm. The contours denote radar reflectivity ($\times 10$ dBz). The bottom figure shows the reflectivity of a pulse storm. Adapted from Chisholm and Renick (1972)

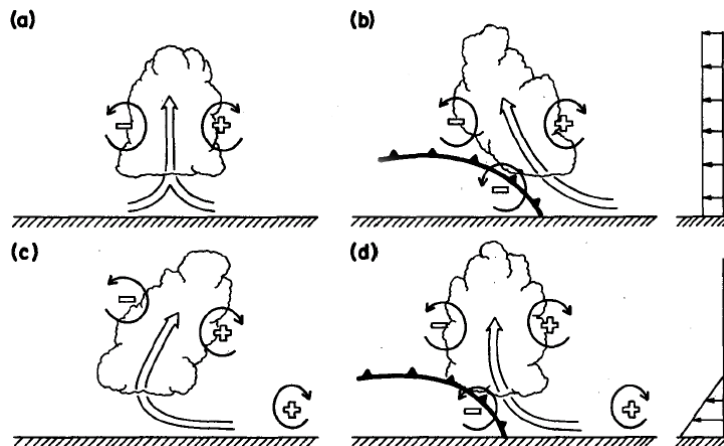


Figure 3.3: Schematic diagram showing how a buoyant updraft may be influenced by wind shear and/or a cold pool. From Rotunno et al. (1988).

most conducive for long-lived squall lines. Numerical simulations of RKW show that in an environment having low-level shear, stronger vertical motions are induced along the leading edge of the cold pool than in a no-shear environment. This can be explained by considering the horizontal vorticity.

Considering an updraft in an environmental flow without any shear (fig. 3.3.a.) we can tell that the horizontal gradient in buoyancy will generate negative and positive horizontal vorticity on the left and right flanks of the updraft respectively. In the center of the updraft there will be no net buoyancy and we can expect an upright updraft to form. This upright orientation is the most optimal for deep convective development, because the lifting will be deepest in this situation (Droegemeier, 1985 according to RKW), so that the air has the biggest chance of reaching its level of free convection (LFC).

When low level shear is present the air that flows into the updraft will already possess vorticity; positive vorticity in the case of fig. 3.3.c. The updraft as a whole will keep this net positive vorticity, which results in a tilted updraft.

When we consider the updrafts that occur along a cold-pool boundary as shown in 3.3.b and 3.3.d, another source of vorticity is important. The horizontal gradient of buoyancy across the boundary gives rise to the formation of negative baroclinic vorticity in the situation of 3.3.b. In a situation with environmental shear this will result in an updraft tilted over the cold pool. RKW noted that the vorticity due to the cold pool can be compensated for by opposite vorticity in the air that is being lifted, as shown in fig. 3.3.d. If this environmental vorticity balances the cold-pool induced vorticity, the resulting lifting will be upright and deep, which will likely enable the air to reach its LFC and promote new deep convective development.

Cell regeneration: Compensating downdraft theory (Lin et al., 1998)

Lin et al. (1998) have developed an alternative theory on cell regeneration based on numerical simulations. In short, this theory states the following: since every updraft is expected to have compensating downdrafts next to it, a new cell can form as soon as the previous cell has moved away far enough from the cold pool boundary so that its compensating downdrafts do not inhibit new convective updrafts there. Lin et al. have found that when storms move away quickly from the boundary, which happens in high-shear environments, new cells form more rapidly after each other. Which of the two theories, that of Lin et al. or RKW-theory describes best what is actually happening is still a subject of debate.

3.2.2 Multicell cluster storms

Often a distinction is made between a *multicell cluster* and *multicell line*, the latter also being referred to as *squall lines*. Generally, multicell complexes are clusters of convective cells in various stages of their life cycles. An important characteristic of multicell complexes is that although their building blocks, single- or ordinary cells, move with the mean wind, the complex as a whole often has a deviation toward the direction where the new cells grow. Compared to single cell storms, multicell clusters have a higher probability of producing severe weather including damaging winds, large hail and occasionally weak tornadoes.

3.2.3 Multicell line storms or squall-lines

When convection is triggered by upward motions in an area having a linear shape, for example a cold front or a prefrontal convergence line, the deep convection that ensues will also be linearly organized. Storms can also become linearly organized due to the merging of their outflows and the resulting formation of one single outflow boundary along which new convective cells are triggered. We will refer to this form of convection as a squall-line or quasi-linear convective system (QLCS).

Radar observations show that the leading edge of a squall-line is usually visible as a narrow band of strong reflectivity. Sometimes this band is continuous and on other occasions it is composed of discrete areas of high reflectivity. In mature squall-lines this zone may be followed by a zone of weaker reflectivities, the *transition zone* and finally a wide zone of higher reflectivities that is referred to as the *stratiform precipitation region*.

The leading high reflectivity zone is caused by the lifting of the air mass present ahead of the line to its LFC. Numerical simulations by many researchers (e.g. Fovell and Ogura, 1989) have shown that the interaction between the mass of evaporatively cooled air – referred to as the *cold pool*– and the environmental wind shear is of crucial importance to the propagation of squall lines.

The Rear Inflow Jet

Apart from the flow of buoyant air from the pre-convective environment, the front-to-rear flow (FTR), within squall-lines generally also a flow develops from rear-to-front (RTF) along the top of the cold pool. This flow is frequently referred to as the *rear inflow jet* (RIJ). The origin of the rear inflow jet lies in a horizontal pressure perturbation gradient that develops at mid-levels in the stratiform precipitation region. This gradient is thought to arise because of a gradient in buoyancy-induced pressure perturbation p'_b under the FTR flow of positively buoyant air (LeMone, 1983). Since any buoyant air will have high and low perturbation pressure p'_b respectively above and below it (compare fig. 2.2), a horizontal gradient of buoyancy within the FTR flow will induce a gradient of the perturbation pressure below it. Given that the air within the FTR is the most buoyant near the leading edge of the squall-line it will induce the strongest negative perturbation pressure there. The horizontal pressure gradient at mid-levels that results from it induces the rear to front flow at mid levels, the rear inflow jet. A rear inflow jet may or may not descend to the surface as it approaches the leading band of upright convection. It is still not well understood when a RIJ will descend and when it remains aloft. If it reaches the surface severe wind gusts may be the result.

Surface pressure field near squall lines

Squall-lines have a very characteristic associated pattern of surface pressure. this is shown in fig. 3.4. The gust front is thought to be dynamically similar to a gravity current (or density current), that occurs when a fluid of high density spreads along the bottom of a basin containing a fluid of lesser density. This implies that we can expect the same pressure perturbation as those associated with a gravity current. The different pressure features are the following.

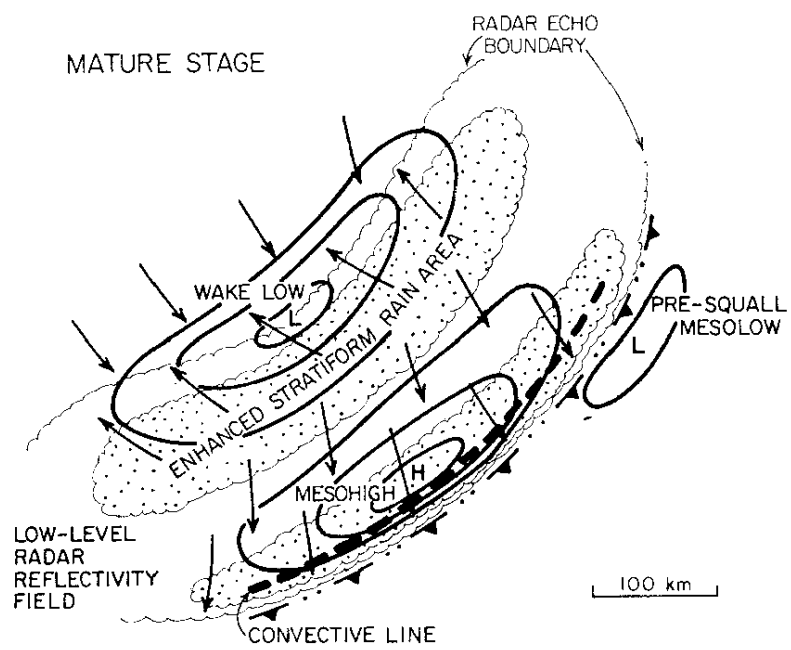


Figure 3.4: Surface pressure field in the vicinity of a squall-line. From Johnson and Hamilton (1988).

Very near the gust front there is a non-hydrostatic ridge of high pressure. This occurs because the fluid ahead of the gust front slows down, which by Bernoulli's equation implies that its pressure should rise. This dynamically induced high pressure area is as large as the area where the winds change direction near the density current. That is a few kilometers at most and therefore too small to recognize on mesoscale pressure analyses. However, on pressure recordings it can often be seen as a spike with an amplitude of a few millibars. Behind the gust front, a larger area of high pressure is present that has a hydrostatic origin: it is a consequence of the greater density of the cold air. Behind this so-called meso-high, a *wake low* may form. This area of low pressure has a hydrostatic nature as well. The wake low is caused by adiabatic warming of air in the rear inflow jet. Within the intense part of the stratiform precipitation region, this warming is (partly) offset by evaporational cooling. Behind the most intensive precipitation cooling is smaller so that the center of low-pressure is observed at the back edge of the system (Wakimoto, 2001).

Bow echoes and Line Echo Wave Patterns (LEWPs)

It is often observed that squall-lines have vortices at their extreme ends, both in environments of low and high environmental wind shear. These vortices are known as *book-end vortices*. Their formation process can be summarized as follows. In a developing squall-line, a cold pool will form that becomes increasingly larger and cooler. The temperature gradient along the cold-pool boundaries causes baroclinic horizontal vorticity to form there, having vortex-lines parallel to the boundary.¹ Air having this sense of vorticity is ingested by the leading convective line. At the line-ends, the buoyancy gradient will have a component parallel to the line (the cold pool is colder near the center of the line and warmer near the line ends) which produces baroclinic vorticity that is not parallel with respect to the leading convective line. This implies that upon ingestion of this baroclinic vorticity by the convective line, tilting of vorticity will occur. In this manner cyclonic vertical vorticity will form at the northern end of the line and anticyclonic vertical vorticity at its southern end. Between the vortices the leading squall-line usually "bulges forward" so that on radar a bow-shaped echo or *bow-echo* appears. It is often observed that after the book-end vortices have formed, the northern vortex will gradually become stronger than the southern vortex. This is caused by the effects of the coriolis force (Weisman and Davis, 1998).

Generally, Doppler-velocity on a PPI-scan shows the approach of the RIJ very clearly. If the squall-line is approaching the radar, it will likely scan through the front-to-rear flow as well as the rear inflow jet. Along their mutual boundary an area of so-called *mid-level radial convergence* (MARC) (Schmocker et al., 1995 according to Weisman, 2001) is usually detected.

In environments of high wind shear, squall-lines also tend to have vortices along the line. They may then consist of multiple bow-echo-like segments (Weisman and Davis, 1998). The squall-line is then referred to as a *line echo wave pattern* (LEWP, see fig. 3.5). The along-line vortices are caused by the tilting of environmental horizontal vorticity (as opposed to the tilting of system-generated vorticity discussed above), similar to the tilting mechanism at work in super-

¹This is the counterclockwise vorticity in fig. 3.3.

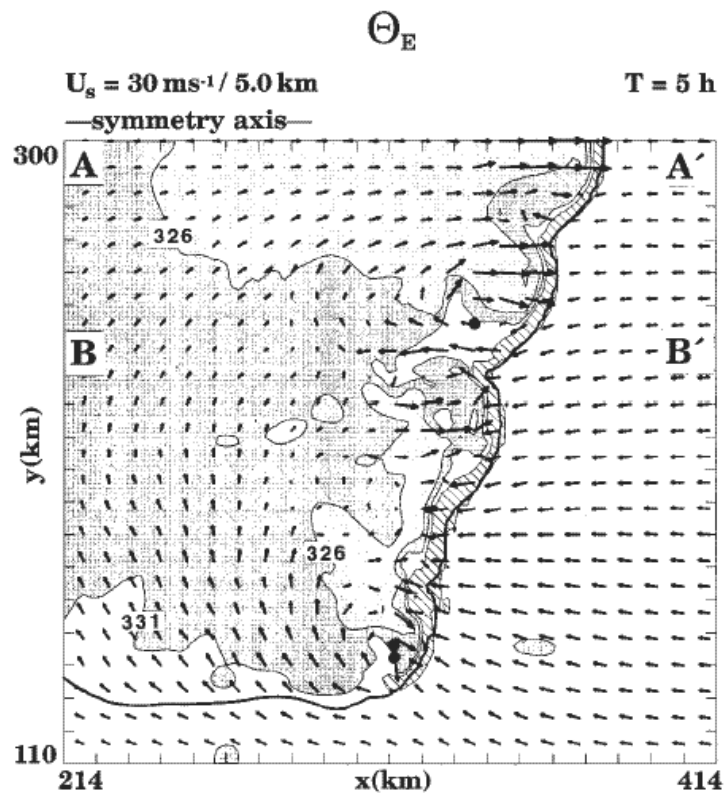


Figure 3.5: Horizontal cross section of system-relative flow and θ_e at 2 km AGL for a squall-line simulation where environmental shear is 30 m/s in the lowest 5 km. The image shows the flow after 5 hours. From Weisman and Davis (1998).

cells (see next paragraph). In fact, if these vortices are strong, one may speak of embedded supercells.

3.3 Supercells

Supercells have a longer lifetime than multicells or single cells. The concept of a supercell was first mentioned in a study by Browning (1964) who described it as being a quasi-steady form of an ordinary cell. Later, the type of storms that were traditionally described as supercells turned out to contain a rotating updraft, commonly referred to as a mesocyclone. Hereupon Browning (1977) redefined a supercell as being a convective storm having a mesocyclonic circulation. In this study we will use a more strict definition that also puts certain constraints on the properties of the mesocyclone. We adopt the definition by Burgess and Doswell (1993) who define a supercell as *a thunderstorm having a deep and persistent rotating updraft*.

Supercells are known for producing severe weather. The main reason for this is that supercells contain very high vertical velocities within both updrafts and downdrafts, which may significantly exceed the vertical velocities predicted by parcel theory. Numerical experiments in the late 1970s and 1980s have provided considerable insight into the dynamics of supercell convection (see Wilhelmson and Klemp, 1978; Rotunno and Klemp, 1981; Rotunno and Klemp, 1984; Weisman and Klemp 1984). Also, some more theoretical studies (e.g. Lilly, 1982; Davies-Jones, 1984) have contributed to the current understanding of supercells.

3.3.1 Dynamics

Supercells occur in an environment characterized by relatively strong wind shear and latent instability. Rasmussen and Blanchard (1998) have shown that radiosondes measured higher wind shear between the boundary layer and 6 km altitude in supercell environments (19.1 ms^{-1}) than in the environments of ordinary cells (10.8 ms^{-1}).

Updraft rotation at mid-levels

Davies-Jones (1984) has shown that positive vertical vorticity automatically becomes correlated with upward vertical motion in certain storm-relative vertical wind profiles. In a mathematical derivation he establishes an expression of their correlation coefficient. The physical interpretation of the theory is the following. We consider an isentropic or pseudo-isentropic surface near a convective updraft depending on whether we consider unsaturated or saturated air. Because (pseudo-) potential temperature is conserved following a parcel trajectory, any vertical motion will displace this surface upward or downward. For example, an initiating convective updraft will cause a local upward displacement of the surface, as is shown in fig. 3.6.

Now we consider any storm-relative horizontal flow that may be present in the isentropic surface. Since the flow must follow the surface, any (storm-relative) horizontal flow will be forced upward on the upwind side of the displacement peak and downward on its downwind side. If there is purely vertical

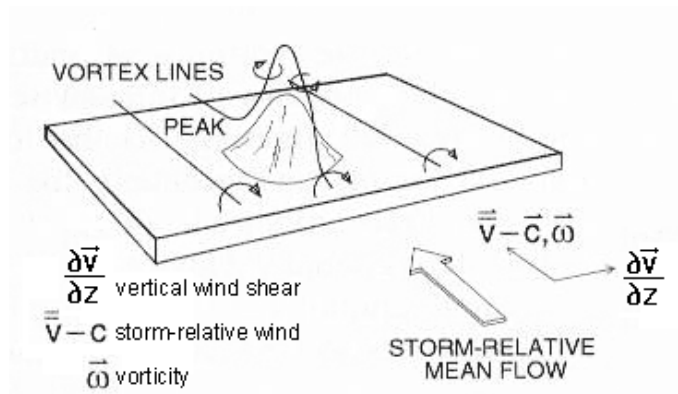


Figure 3.6: Physical interpretation of how a correlation develops between vorticity and vertical motion. Based on a figure from Davies-Jones (1984).

wind shear at the location of the surface, this may be represented by vortex lines lying within the surface. Potential vorticity $\boldsymbol{\omega} \cdot \nabla \theta$ is conserved following an isentropic surface. Therefore any vortex line that initially lies in a surface, which implies zero potential vorticity, must remain within that surface. The vortex lines may have a component parallel to the storm relative wind (as in fig.3.6) which is called *streamwise vorticity*. When this is the case, the vortex lines must be tilted into the vertical near the displacement peak, which results in vertical vorticity at both the upwind and downwind sides of the displacement peak.

An important observation is that if horizontal storm-relative winds are present, the largest vertical motions are not located at the location of the largest displacement, but upstream of the peak. This implies that there is a positive correlation of upward vertical motion and cyclonic vorticity.

Helicity and hodographs

The tilting of streamwise vorticity can be quantified by the so-called storm-relative helicity (SRH). SRH is the product of the storm-relative inflow and the streamwise vorticity integrated over a layer that is thought to form the source of the storm inflow. Mathematically, SRH is defined as

$$SRH = \int_{SFC}^{top} |\mathbf{v} - \mathbf{c}| \omega_{streamwise} dz = \int_{SFC}^{top} \boldsymbol{\omega} \cdot (\mathbf{v} - \mathbf{c}) dz. \quad (3.1)$$

For *top* usually a height of 3 or 1 km AGL is chosen. Studies (e.g. by Rasmussen and Blanchard, 1998) reveal that supercells tend to occur with large 0–3 km SRH. 0–1 SRH km has recently been recognized as being a parameter of importance to the genesis of supercell tornadoes (Rasmussen, 2002; Monteverdi et al., 1994). An alternative formulation of SRH that assumes there are no vertical velocities outside of the updraft, which is a reasonable approximation, is as follows:

$$SRH = \int_{SFC}^{top} \frac{\partial \mathbf{v}_h}{\partial z} \times (\mathbf{v}_h - \mathbf{c}) dz, \quad (3.2)$$

where \mathbf{v}_h is the horizontal wind. This formulation is particularly of use, because it enables us to assess SRH from a hodograph. A hodograph is a parameter curve $\mathbf{v}(z) = (u(z), v(z))$ in the x,y-plane that can be thought of as the curve swept out by the tip of the horizontal wind vector while it is being evaluated at increasing altitudes. The vertical shear vector $\mathbf{v}_h(z) = \frac{\partial \mathbf{v}}{\partial z}$ is by definition tangent to the hodograph. Vector calculus shows that for a hodograph (that does not intersect itself) and a storm moving to the right of the mean wind shear, the *SRH* equals half the area bounded by the hodograph and the surface and top storm-relative wind vectors drawn from the tip of the storm motion vector. It is obvious that SRH is highly dependent on the storm motion vector. The storm motion can be deduced from radar data or estimated beforehand. Some empirical formulas have been developed to do this, the best of which is the ID-method (Bunkers et al., 2000):

$$\mathbf{c} = \mathbf{v}_{mean} + D \left(\frac{\mathbf{v}_{shear} \times \hat{\mathbf{k}}}{|v_{shear}|} \right) \quad (3.3)$$

where v_{mean} is the 0-6km mean wind vector, and v_{shear} is the 0-6km mean wind shear vector. D is an empirical constant of 7.5 m/s. The formula is valid for storms moving to the right of the mean wind shear. If updraft propagation to the left of the mean-wind shear is expected or observed, one should replace the + by a - in the formula.

Low-level updraft rotation

Rotunno and Klemp (1984) show that tilting of streamwise vorticity can explain updraft rotation at mid-levels, but low-level rotation has – at least in part – a different origin. Interpretation of the results obtained by their numerical model has shown that low-level rotation is mainly caused by tilting of baroclinically induced horizontal vorticity into the storm’s updraft. This baroclinically induced vorticity is formed along the storms cold-pool boundary. In many cases the trajectories of parcels that end up in the updraft go through this baroclinic zone and develop horizontal vorticity that upon tilting and stretching into the storm’s updraft can produce low-level rotation.

3.3.2 Radar characteristics of supercells

Supercells have a distinct reflectivity pattern on radar. One of the most important features is the bounded weak echo region (BWER) that corresponds with the lower and central parts of the updraft. It is a region of low reflectivity because only small cloud droplets are present in the updraft that are carried upward before they can grow into rain droplets or hailstones by coalescence and the Bergeron process. At high levels, where the updraft speed gradually diminishes there is high reflectivity. The region of high reflectivity reaches the surface in the downdraft regions that is located downshear. The highest reflectivities are located very near the updraft where the largest hailstones fall.

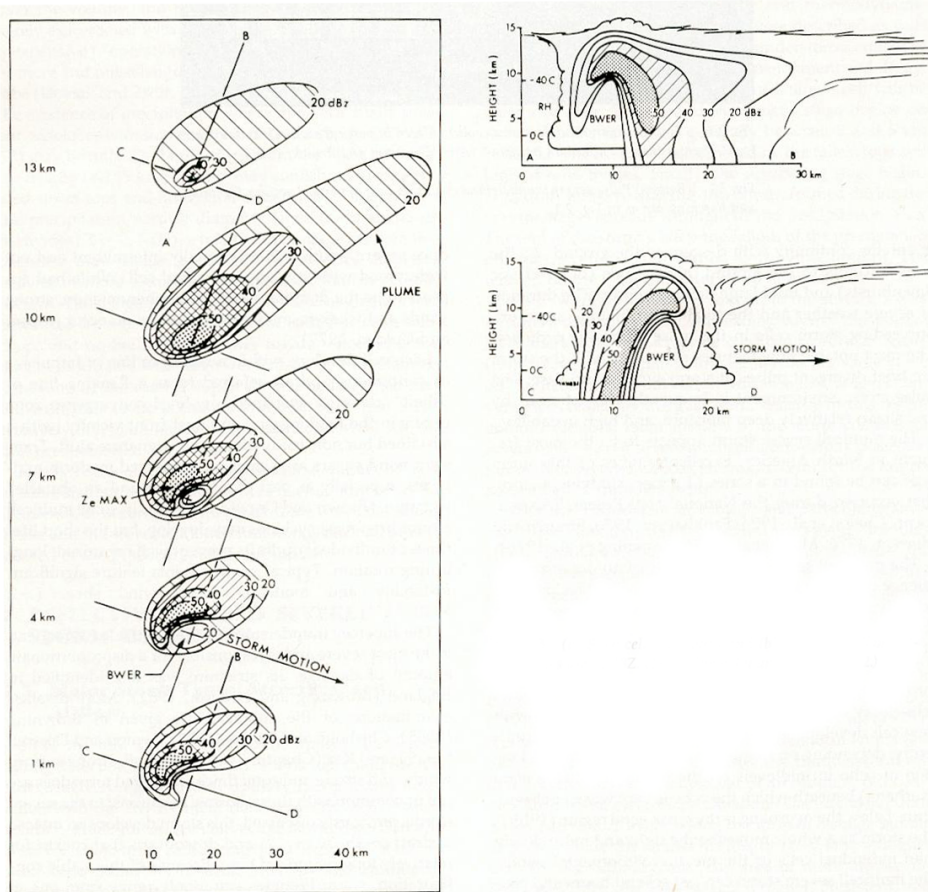


Figure 3.7: Radar plan view of a supercell storm at 1, 4, 7, 10 and 13 km AGL, and vertical sections of the storm along A-B and C-D. Reflectivities in dBZ. (from Chisholm and Renick, 1972)

Smaller hailstones and rain, having lower fall velocities, are farther displaced from the updraft when they reach the surface than their heavier counterparts. This effect is often referred to as the precipitation cascade. Because the best scatterers are located very near the (almost) echo free updraft region, a very high reflectivity gradient is visible on a PPI scan (see fig. 3.7.). Most of the precipitation is carried downshear and by evaporational cooling of the air a strong downdraft is formed, called the forward flank downdraft (FFD). The cyclonic mid-level vortex has the effect of carrying the precipitation in a clockwise manner around the updraft, which may result in a so-called hook-echo, a cyclonically curved appendix on the upwind side of the echo that is most prominently seen at low levels. Evaporational cooling of precipitation in combination with certain dynamic effects (that are not yet fully understood), the so-called rear flank downdraft (RFD) forms. Doppler radar adds a new dimension to severe storm detection. Supercells can be distinguished by their mesocyclone that is detected by Doppler radar as a dipole of inbound and outbound velocities with its axis parallel to the radials (see Section 4.2.3.).

Variations in supercell morphology

Supercells can differ greatly in appearance. There are four sub-classes of supercells: High-Precipitation supercells (HP), Classic supercells (CL), which we have described above, Low-Precipitation supercells (LP) (Bluestein and Parks, 1983), and Mini-supercells (MS). We will describe HP- and mini-supercells here in short.

HP-supercells

A typical characteristic of a HP storm (Moller et al., 1990), is that much of the precipitation is reingested by the updraft. A large part of the precipitation falls on the up-shear side of the storm causing the radar echo to show a kidney-bean shape. HP supercells sometimes produce tornadoes and large hail. Their main threats consist of flash flooding and severe downburst winds. The differences between LP-, classic and HP-storm types are thought to be mainly a result of difference in storm-relative winds at the storms anvil-level (Rasmussen and Straka, 1998), though microphysical processes may also play an important role.

Mini-supercells

Mini Supercells (MS) (Burgess and Lemon, 1991; Burgess et al., 1995) are also known as low-topped supercells and are characterized by a smaller horizontal and vertical extent than other supercells. MS storms resemble their larger counterparts in all aspects but their size. This means that they are hard to detect at a large distance from the radar (Grant and Prentice, 1996).

They usually occur in environments of relatively low latent instability, low equilibrium levels and in strong low-level shear. Though absolute CAPE values are often found not to be high near MS storms, there is usually a relatively large amount of CAPE present in the lowest kilometers of the atmosphere. Modeling studies by Wicker and Cantrell (1996) found that low-level CAPE (i.e. CAPE located in the lowest 1–3 km) appeared to be more important for the development of rotational characteristics within MS storms than larger values of CAPE through a deeper layer.

Given that The Netherlands and its surroundings experience many occasions of high wind shear while high CAPE is rare, future research may well find this type of supercell to be the most common in this part of Europe. This hypothesis is supported by studies on tornadic MS storms in California and southern Australia (Monteverdi and Quadros, 1994; Monteverdi et al. 2000, Hanstrum et al., 2000) that occur in thermodynamic environments (described above) not uncommon for The Netherlands.

Chapter 4

Doppler Radar

4.1 Principles of a radar

A radar is a device that transmits and receives radio frequency electromagnetic waves. A small part of the emitted radiation can be scattered back to the radar by particles in the atmosphere. From the time it takes before the radiation has returned, the distance of the particles can be determined. Because water droplets and – to a somewhat lesser extent – ice-crystals are scatterers of the radiation, a radar can be used to detect precipitation. From the amount of radiation that is returned from a particular volume of air, the reflectivity of that volume can be determined, which is dependent of the number and size of reflecting particles contained within it.

The dominant scattering process is usually so-called Rayleigh scattering. This occurs when the diameter of the scattering particle $d < \lambda/10$, where λ is the wavelength of the radar signal. For scattering by spherical particles, the amount of scattered radiation is proportional to the sixth power of its diameter, that is

$$\sigma \propto \frac{d^6}{\lambda^4} \quad (4.1)$$

The reflectivity Z of a volume containing scatterers is

$$Z \equiv \frac{1}{\delta V} \sum_n d^6 \quad (4.2)$$

We assume that raindrops are roughly spherical so that for the KNMI C-band radar, that emits 5.3 cm-wavelength radiation, raindrops (which are smaller than 0.5 cm) fall in the Rayleigh regime. Hailstones or large snowflakes scatter the radiation differently. They fall in the so-called Mie or resonant region, where the scattering cross-section is given by a more difficult function of d .

4.2 Principles of a Doppler-radar

In addition to determining position and reflectivity, a Doppler radar can also detect the speed at which the ensemble of particles is moving from or toward the

radar. This is done by measuring the phase difference of the transmitted and received radiation. When a phase difference of, say, ϕ is measured, this means that the pulse has traveled a distance of $\lambda(n + \frac{\phi}{2\pi})$, where λ is the wavelength of the emitted pulse and n is an unknown integer. The distance of the ensemble of particles that scattered the pulse¹ is half that distance, $x = \frac{\lambda}{2}(n + \frac{\phi}{2\pi})$. By measuring the change in phase difference between two separate transmitted and reflected pulses, we can measure the difference in distance of the reflecting particles between the time of the two pulses. $\Delta x = \lambda \frac{\Delta\phi}{4\pi}$. This, only works if the phase change is small, $-\pi < \Delta\phi < \pi$. Dividing the distance difference by the time between the two pulses called the *pulse repetition time* (PRT), gives us the velocity component of the scattering particles with respect to the radar:

$$v = \frac{\lambda}{PRT} \frac{\Delta\phi}{4\pi} = \lambda PRF \frac{\Delta\phi}{4\pi}, \quad (4.3)$$

where PRF is the *pulse repetition frequency* $= \frac{1}{PRT}$. The constraint $-\pi < \Delta\phi < \pi$ implies there is a maximum velocity that can unambiguously be detected. From eq. 4.3, it can be seen that the maximum unambiguous velocity v_u is

$$|v_u| = \frac{\lambda PRF}{4}. \quad (4.4)$$

We wish to have a high maximum unambiguous velocity in order to be able to detect large wind speeds. We see that increasing the PRF will give us a higher v_u . However, increasing the PRF will limit the unambiguous range of the radar. This can be understood by noting that the radar has to have received a pulse before transmitting the next. This means that the pulse cannot travel farther than the product of the speed of light and the pulse repetition time. The maximum unambiguous range of the radar is, again, given by half this value. That is

$$r_{max} = \frac{cPRT}{2} = \frac{c}{2PRF}. \quad (4.5)$$

The product of the range and the maximum unambiguous velocity is dependent on the radar's wavelength only:

$$v_u r_{max} = \frac{\lambda c}{8} \quad (4.6)$$

4.2.1 Dual-PRF and unfolding

For this study, data were available collected with the KNMI C-band Doppler radar located at De Bilt (52.10 N, 5.17 E). This radar has a beam width of about 1° . Having a wavelength of 5.3 cm, when a typical range of 200 km is selected the unambiguous velocity is 10 ms^{-1} . Since this is too low to be of use in typical meteorological circumstances, the radar uses the so-called dual-PRF technique by which the unambiguous velocity can be increased. The dual-PRF technique uses two different PRF's in the velocity measurement.

¹Multiple particles at different distances contribute to the reflection of the pulse. However, the scattered radiation is detected as one pulse having one particular phase.

Firstly, a high and a low PRF are used to obtain two different velocity measurements, v_h and v_l , that may or may not be folded outside their respective unambiguous velocity intervals. From their difference it can be inferred how many times the velocities are folded, so that the real velocity can be retrieved. To be more precise, when using two PRF's related by

$$\frac{PRF_h}{PRF_l} = \frac{N+1}{N}, \quad (4.7)$$

a first-guess estimate of the unfolded velocity can be obtained from

$$v = (N+1)v_l - NV_h. \quad (4.8)$$

This unfolded velocity estimate cannot be used as such, because it is quite inaccurate. This occurs because the variance of the original estimates adds up as $\sigma^2 = (N+1)\sigma_l^2 + N\sigma_h^2$. However, it is a useful quantity for determining how many times the original measurements are folded so that they can be unfolded.

It can be shown that this technique can extend the effective unambiguous velocity interval to

$$v_{u,eff} = \frac{v_{u,h}v_{u,l}}{v_{u,h} - v_{u,l}}. \quad (4.9)$$

The elevation is the angle between the direction of the radar beam and the horizon. The azimuth is the horizontal direction of the radar beam expressed with respect to true north. Every sample of data retrieved at one particular azimuth is called a ray. The radar scanned 360 rays at each elevation, the rays all being spaced 1° . Then it repeats this at another elevation. The radar was programmed to make a complete volume scan every 15 minutes, comprised of scans at ten elevations: 0.5° , 2.0° , 3.5° , 5.0° , 7.0° , 9.0° , 12.0° , 15.0° , 20.0° and 25.0° . For the volume scans, the radar in De Bilt uses a high PRF of 1000 Hz and a low PRF of 750 Hz. By eq. 4.4 the associated unambiguous velocities are 13.3 m/s and 10.0 m/s respectively. The dual-PRF technique increases the unambiguous velocity to 39.9 m/s. The associated range of the radar is 150 km.

4.2.2 De-aliasing

The dual-PRF technique is implemented in a special way on the KNMI-radar, because of the characteristics of the signal processing hardware: the PRF is switched between the high (1000 Hz) and low (750 Hz) PRF every ray. The first-guess velocity, that determines the how the velocity must be unfolded, is constructed from the low (or high)-PRF measurement of the current ray and the high (or low)-PRF measurement of the previous ray. This technique works quite well, but on zones of extremely high azimuthal shear of the radial wind, the velocity may be unfolded into the wrong Nyquist interval. Occasionally, unfolding errors also occur elsewhere. A so-called dealiasing algorithm described by Holleman and Beekhuis (2003) removes most of these errors from the data, but does not remove all errors. Since the algorithm is based on comparing the unfolded velocities of neighboring points with each other, most of these remaining errors are located near the boundaries of groups of data points and areas of no data.

There other consequences of the described way of operating the radar. A clutter filter is used that removes any signals that are believed not to be caused

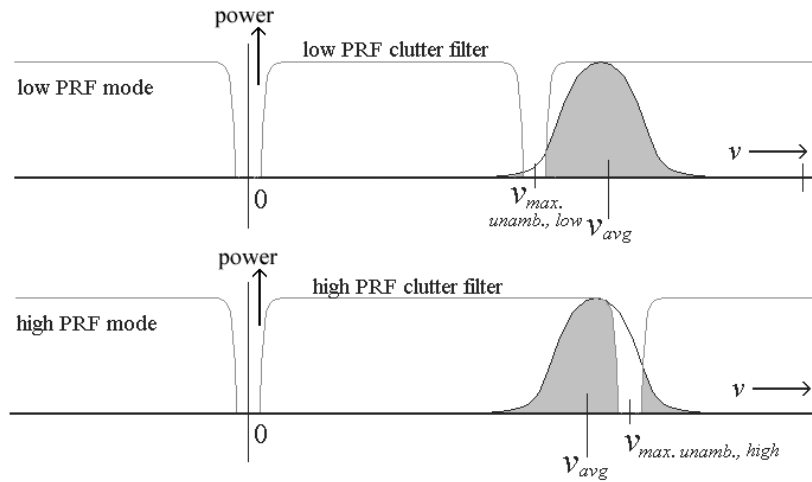


Figure 4.1: Example of different filtering of the weather signal by the high and low PRF filters.

by meteorological phenomena but by clutter, side-lobes, anomalous propagation or other sources. This is done by removing the returned signals having a phase-difference corresponding with zero velocity. The idea behind this is that most of the unwanted signals originate from objects having zero velocity with respect to the radar. However, if signals with zero velocity are to be removed, signals corresponding with $2N$ times (where N is a signed integer) the unambiguous velocity interval are also removed, since these cannot be distinguished (see fig. 4.1). This means that the power of such signals will be lower than the true value. Because the unambiguous velocity changes each ray as the radar is switched between low and high PRF, the filter changes as well. This means that different parts of the returned weather signal may be removed by high PRF filter than those removed with the low PRF filter. This may cause the detected returned power to fluctuate every ray since more power may be filtered away by one filter than by the other. There is also an effect on the measured Doppler-velocities. Since the high PRF filter may remove one wing of the signal pulse, while the low PRF filter removes the other, the average velocity of the signal may fluctuate as well. These effects can clearly be seen in the reflectivity and velocity images shown in the next chapter. A new generation of signal processors is planned to be installed with the KNMI radars, that will not filter the signal away but rather make a linear interpolation of the signal around 0 velocity (dashed line in fig. 4.1). This solves the problems of the fluctuating power and velocities for a great part.

4.2.3 Detection of mesocyclones

A mesocyclone can be detected by radar. It will be visible as a strong azimuthal gradient of radial velocity. For (anti)cyclonic mesocyclones (in the northern hemisphere), one would expect to observe motion away from the radar to be located to the right (left) of winds having a component toward the radar,

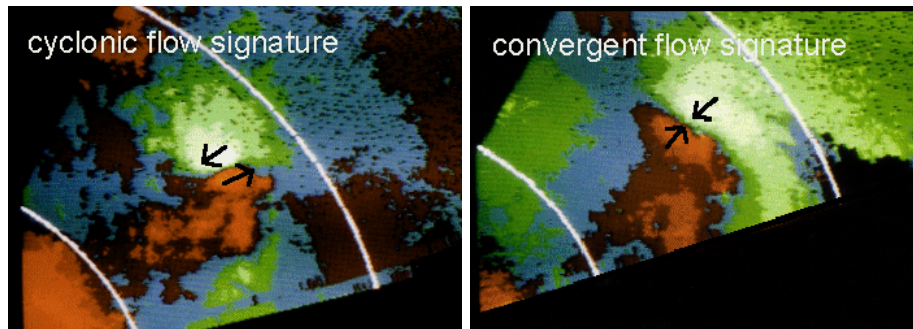


Figure 4.2: Signature of a cyclonic (NH) mesocyclone (left) and a signature of convergence (right). Based on a figure from Doviak and Zrnić (1993).

as shown in the left part of fig. 4.2. The right part of the figure shows a strong gradient of radial shear of radial velocity. Close to the radar velocities are directed away from the radar, while at greater distance the velocity has a component toward the radar. This is a signature of convergence. Divergence (e.g. in a downburst) has the opposite signature of convergence. Combinations of con/divergence with (anti)cyclonic rotation are visible as a combination of azimuthal and radial shear.

One speaks of a mesocyclone when (Moller, 2001):

- the core of the detected rotation (that is the part that is in solid body rotation) is smaller than or equal to 10 km,
- the range-dependent rotational velocity equals or exceeds the strength shown in fig. 4.3,
- it has a vertical extent of at least 4 km,
- it persists for at least 15 min.

It should be noted, however, that when the distance to the radar is large, average velocities of a large sample volume are measured. Similar mesocyclones will therefore seem to have smaller shears at larger distances from the radar. This effect is compensated for in fig. 4.3. If the size of the sample volume is larger than the size of the mesocyclone, it will not be detected at all.

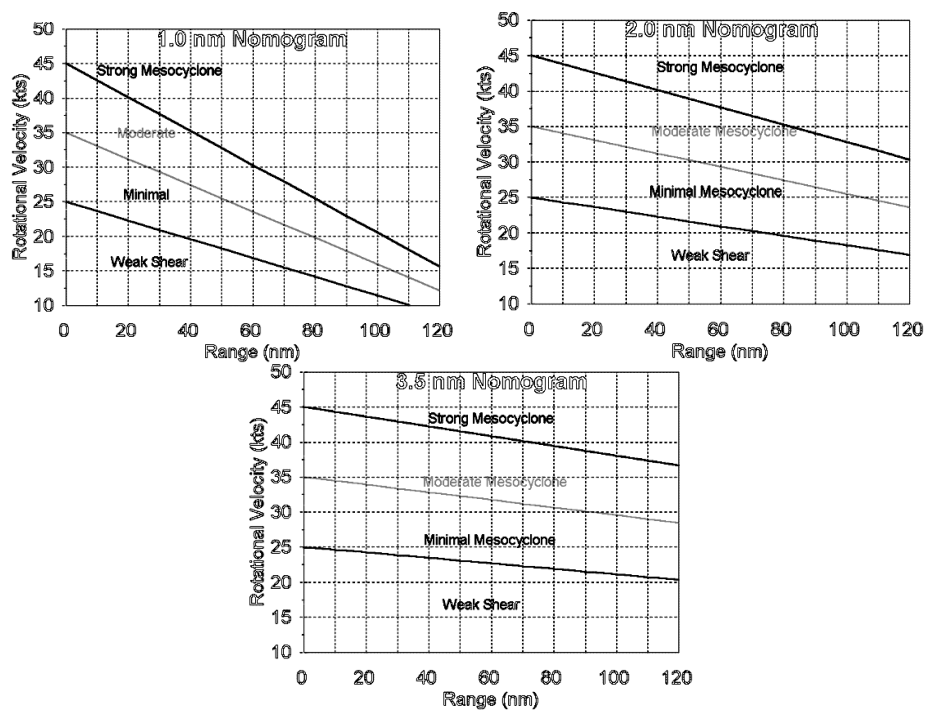


Figure 4.3: Nomograms in use at the National Weather Service to determine the strength of mesocyclones observed with a WSR-88D radar.

Chapter 5

Cases

The following map shows the area where the cases discussed below have occurred.

5.1 A squall line in winter, January 28 2003

5.1.1 Event description

In the afternoon January 28th, 2003, a squall-line formed over the Southern North Sea and moved inland over the southern half of The Netherlands and parts of Belgium. The SAFIR lightning detection system recorded high lightning activity for the time of the year. Severe wind gusts of around 31 m/s were observed at a number of stations just off the Dutch west coast. At one station a gust as high as 39 m/s was measured. As the squall-line moved inland, its precipitation of mostly rain and graupel gradually changed to snowfall.

5.1.2 Synopsis

An upper air analysis of the 28th of January at 12 UTC (fig. 5.2) shows a strong west to northwesterly polar jet over Great Britain, Germany, The Benelux countries and France. At 500 hPa, wind speeds were around 30–35 m/s over much of northwestern Europe. An embedded jet streak was present over Ireland and Southern England with speeds over 40 m/s. At 300 hPa the jet streak core is analyzed further to the south over central France with a wind speed of 50 m/s measured in Lyon. The Benelux countries are in a polar air mass north of a frontal zone over central France and southern and eastern Germany (fig. 5.3). There are only small temperature gradients at low levels. At 500 hPa, there is strong cold advection near the frontal zone over eastern Germany. Over the southern North Sea and The Netherlands some slight cold advection is taking place which has a destabilizing effect on the air-mass. A subtle shortwave trough located over the central UK is evident on the 500 hPa map. It is likely that rising motions caused by advection of cyclonic vorticity at mid-levels ahead of the trough have played an important role in initiating and sustaining the convective system.



Figure 5.1: Map with topographical names referred to in this chapter.

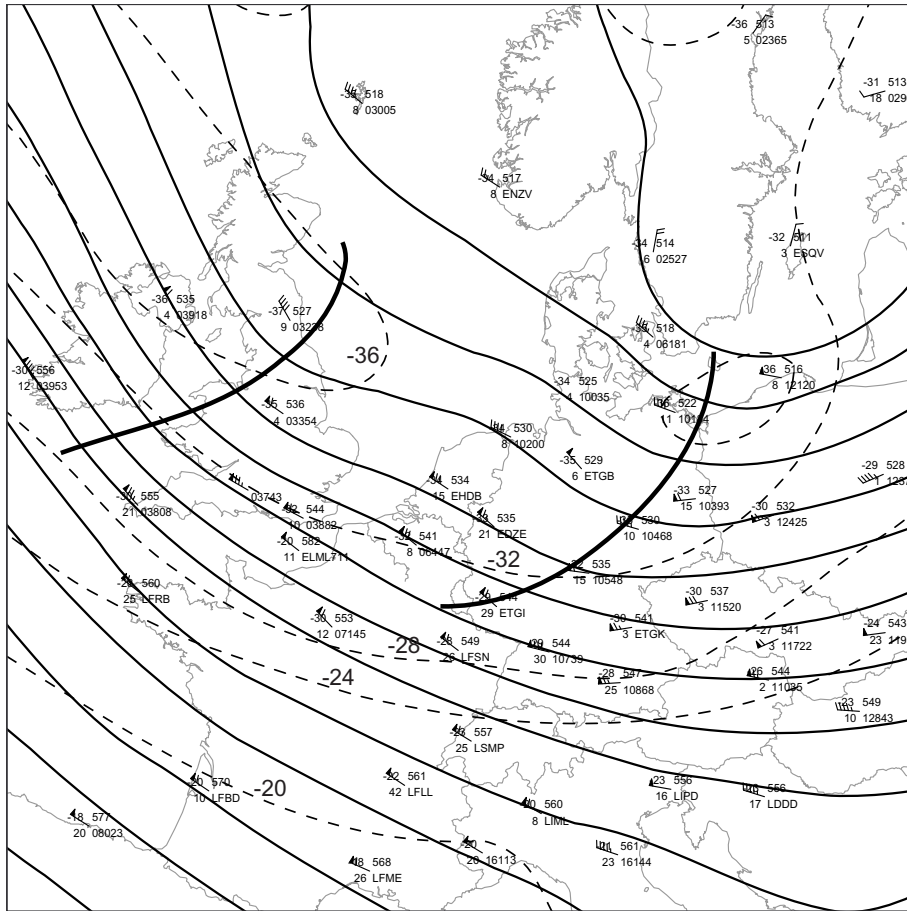


Figure 5.2: Observation plots and analysis by the author of the 500 hPa surface on 28th of January 2003 at 12 UTC. The solid lines are geopotential height contours drawn every 5 gpdam. The dashed lines are isotherms drawn every 4 °C. The thick lines are shortwave troughs. Station plots consist of a conventional wind-vane, temperature (in °C, top left), dew point depression (in °C, bottom left), geopotential height (in gpdam, top right) and WMO or ICAO identifier (bottom right).

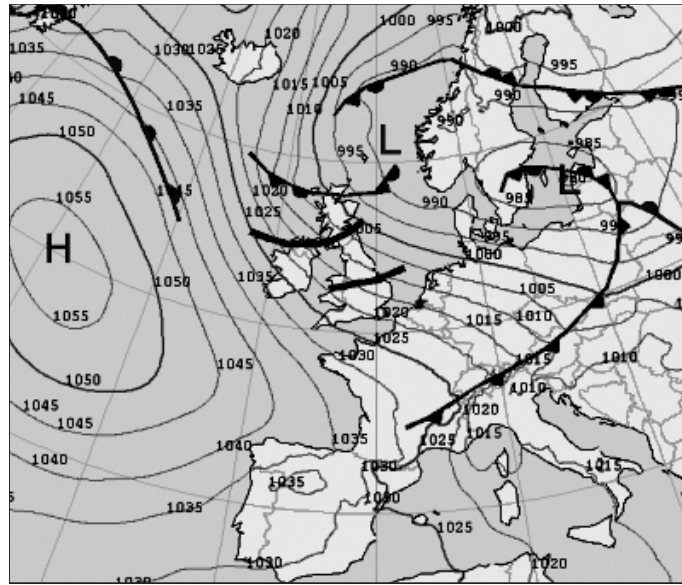


Figure 5.3: Surface analysis at 28 January 2003 12 UTC. Source: KNMI.

Instability

We assume that the sounding from De Bilt taken at 12 UTC (see fig. 5.4), approximately 4 hours before the squall-line arrived, is fairly representative of the environment ahead of the squall-line. This sounding shows a well-mixed boundary layer from the surface up to approximately 930 hPa. Above this altitude the profile is nearly saturated up to 850 hPa. At 850 hPa the temperature rises a degree or two and the air becomes a bit drier. The air is dry and conditionally unstable up to 660 hPa and above that it is slightly stable. Around 530 hPa the air becomes much drier and stable up into the stratosphere.

By plotting a parcel ascent curve, we can see that only very low CAPE is available, approximately 40 J/kg. This value should not be taken too literally. If, for example, the measured dew point temperature in the parcel source layer were a few tenths of °C lower, there would have been no CAPE at all. A dew point temperature a few tenths higher would have doubled the amount of CAPE. Since this is within the range of measurement errors and variability on the scale of kilometers or less, the only conclusion that can be drawn from this measurement was that CAPE was likely very small at the time of measurement. More CAPE can have been building up during the four hours before the passage of the squall line. In contrast to warming at low levels, which is typical of most summertime thunderstorm situations, cooling of mid-levels has been mainly responsible for destabilisation in this case. There is no indication of any warm advection at low levels and the extensive cloud cover ahead of the system did not allow for significant solar heating. A slight cold advection at mid-levels can be diagnosed from the 12 UTC map. Furthermore, it is likely that ascent of air at mid-levels ahead of the trough has caused some cooling at as well, leading to further destabilisation. An exact estimate of the CAPE in the immediate

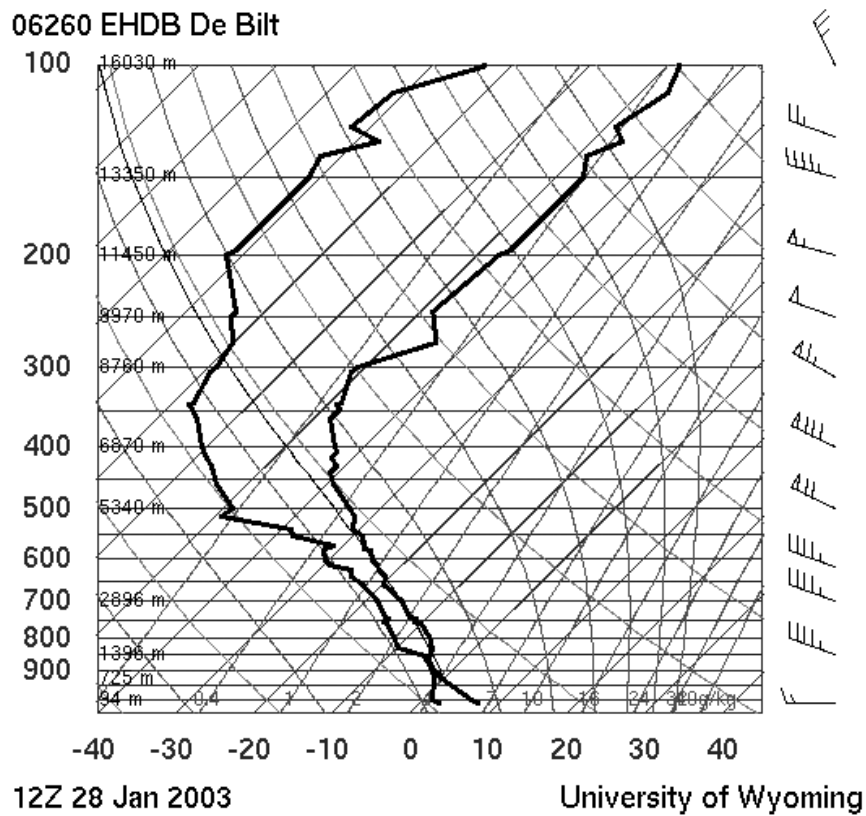


Figure 5.4: Skew-T log-p thermodynamic diagram showing sounding of 12 UTC, January 28th 2003 at De Bilt. A parcel consisting of air mixed over the lowest 50 hPa has a CAPE of 40 J/kg. Source: University of Wyoming.

vicinity of the convection cannot be given. However, it is not likely that CAPE was higher than a few hundred J/kg. Also, it may be possible that only the release of latent instability (as is measured by CAPE) but some other *dynamic* mechanism contributed to the strength of the system.

Wind shear

The event took place in an environment of large wind shear. The 12 UTC sounding at De Bilt shows 15 m/s westerly winds just above the surface. From 900 hPa upward to 600 hPa, the winds are 20 to 25 m/s from a west northwesterly direction. Above 600 hPa winds show a further increase to 43 m/s from the west northwest at 400 hPa. The hodograph that can be constructed from these measurements is shown as a red line in fig. 5.5.

Doppler-radar derived winds (Holleman, 2002) can help us to get a better idea of the flow ahead of the squall-line. These winds measurements, that are available up to a height of 4 km AGL are also shown in fig. 5.5 as a blue line. Above 4km, the Doppler hodograph has been connected to the radiosonde hodograph. Assuming that there was little change of upper-level winds ahead of the storm, this gives us a more representative wind profile. Note that the low-level winds have a more southerly direction ahead of the squall-line.

Wind measurements

As the squall-line passed, strong wind gusts were measured at a number weather stations located just off-shore. The highest observed wind gusts during the passage of the squall-line are shown in fig.5.7. The highest wind gust of 39 m/s was measured at station 06209 (IJmond) between 1500 and 1510 UTC. Other stations along the coast measured lower wind gusts: around 20 m/s along the coast of Zuid-Holland and gusts of up to around 30 m/s along the coast of Zeeland. At station 06316 (Schaar), there was likely some damage to the measuring equipment since the station did not report sensible data after registering a gust of 28 m/s, so it might be that higher gusts occurred here as well. The wind measurements of five stations are shown in fig.5.6. It can be seen that the squall-line produced a very distinct spike in the wind velocity at all of the shown stations and the stations of Brouwershaven and Vlakte van de Raan detect a strong veering of the wind at the moment the highest gusts are measured.

5.1.3 Radar data

The first scan that reveals a large part of the squall-line is performed by the Doppler-radar in De Bilt at 1409 UTC. An image constructed from six sequential 0.5° elevation scans is shown in fig.5.8. We can therein follow various "features" within the reflectivity pattern as they move inland. Also, the formation of bow-shaped structures in the southwest is well visible. At 1509 UTC the system is located from just west of Zeeland over parts of Noord- and Zuid-Holland to the Markermeer.

Some remarkable features are visible on the 0.5° elevation scan. Firstly, there is a 50+ dBZ core visible about 20 km west of Europoort (labeled A). This intense cell can be seen propagating northeastward ahead of the line and

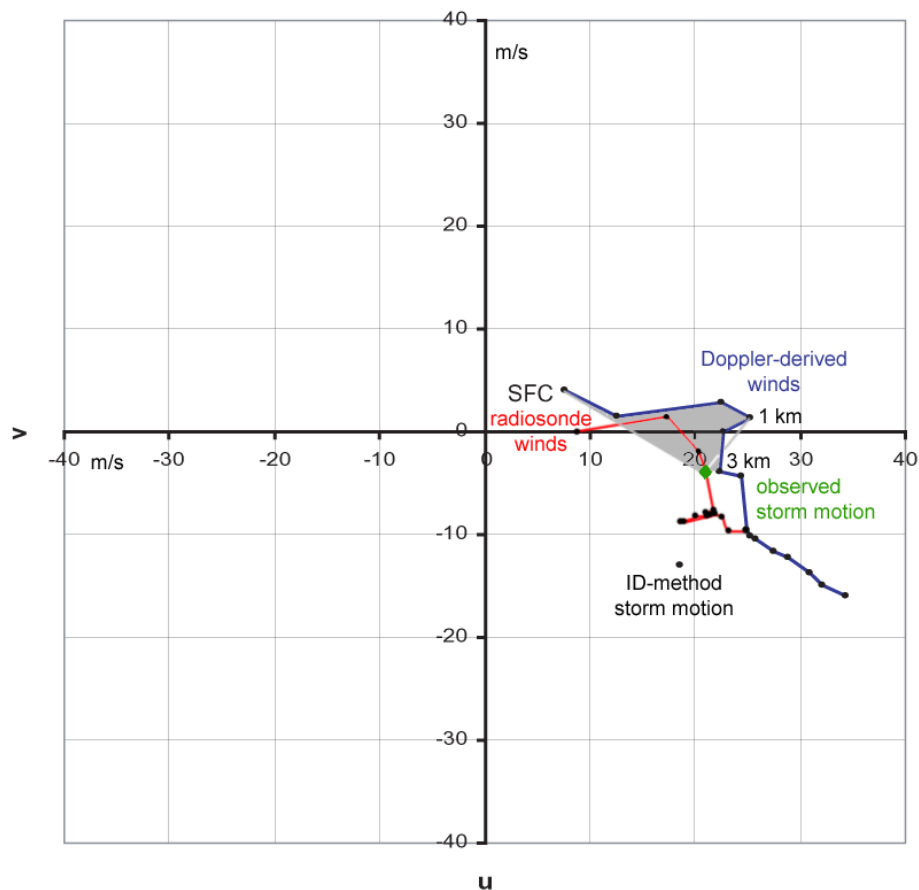


Figure 5.5: Hodograph from radiosonde observation in De Bilt, January 28th 2003 at 12 UTC (red) and from Doppler data at 16 UTC (blue). The observed storm-motion is marked with a green diamond. The ID-method storm motion is marked with a black dot. The grey area is the surface that can be thought of to represent the amount of 0-3 km storm-relative helicity. The added grey/white line marks the limit of the area representing 0-1 km S.R-helicity.

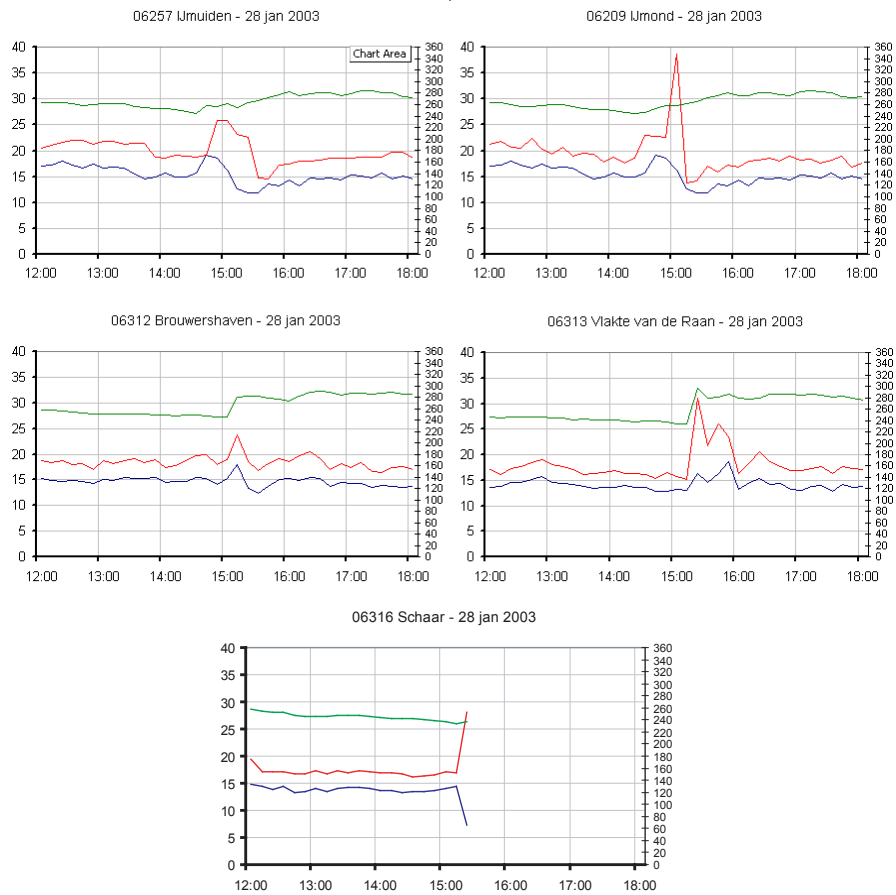


Figure 5.6: Wind measurements at five stations. The green line is the wind direction (degrees), the red line is the maximum 10-minute gust (m/s) and the blue line is the 10-minute averaged wind speed (m/s).

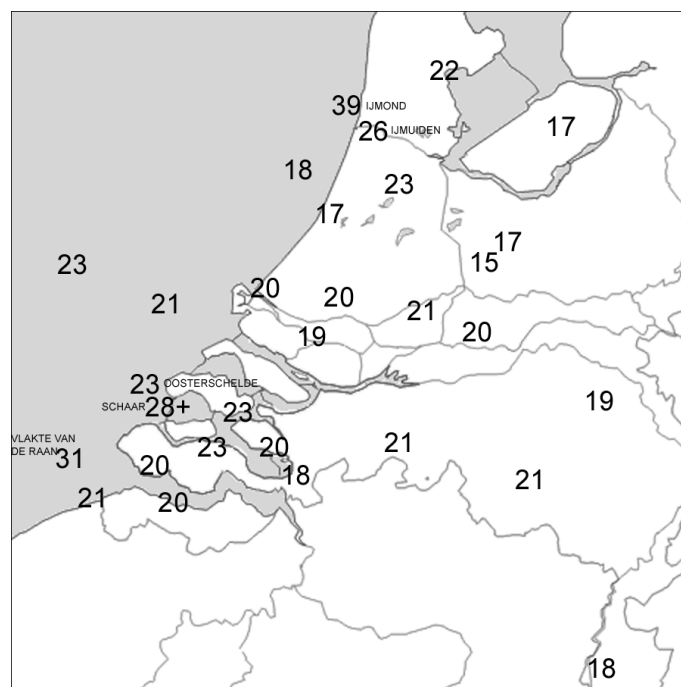


Figure 5.7: Highest observed wind gusts (m/s) during passage of the squall-line on 28th January 2003.

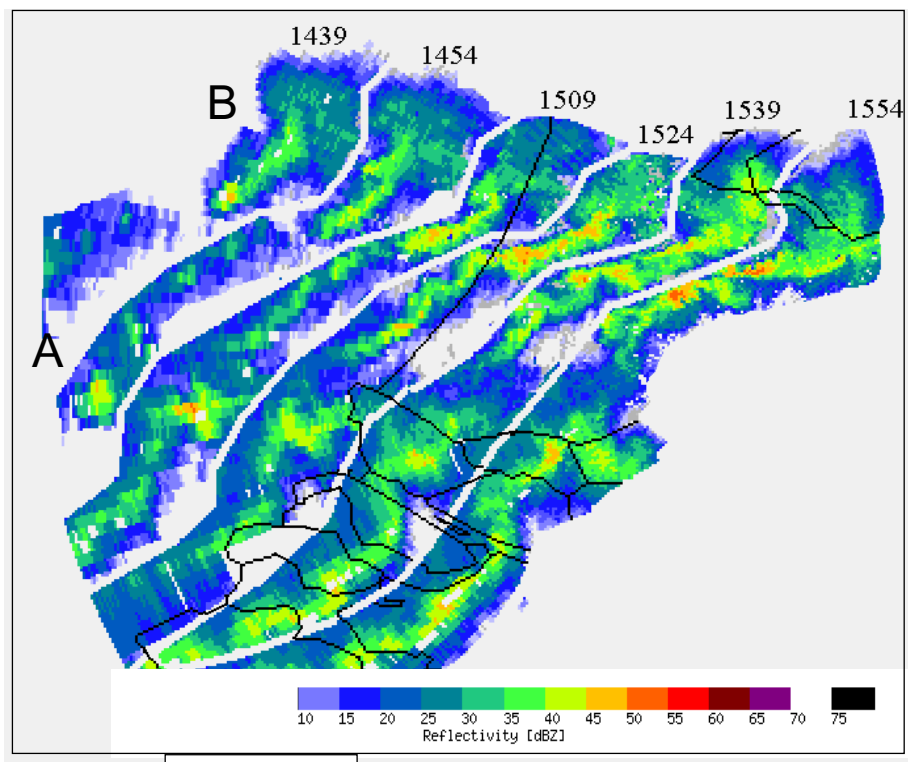


Figure 5.8: Fragments of six sequential 0.5° elevation scans from De Bilt on 28 January 2003 combined in one image.

later becomes a part of the line. It has a deviant motion with respect to most other echoes having a more southerly motion. Interestingly, this reflectivity core has a zone of low reflectivity on its northwestern flank (around 5-10 dBZ). The low-reflectivity is not caused or significantly enhanced by attenuation, since there are no areas of high reflectivity on the same radial that may have caused blocking of the radar signal. The low-reflectivity area can therefore be assumed to be “real”. Its origin is uncertain, but may possibly be associated with a downdraft wind. Another feature (B) is located more northward just off the coast of southern North-Holland. This feature also has a clear reflectivity gap on its rearward side, which gives it a comma-like shape.

Doppler data

Velocity data from the Doppler-radar shows interesting features as well. Doppler-velocities from a 2° elevation scan, of which a mean wind has been subtracted, are shown in fig.5.9. The comma-like feature (B), that first becomes visible at 1439 UTC and has decayed at 1609 UTC, seems to be associated with areas of very high radial shear numbered 1 and 4. Velocities from the lowest elevation PPI scan, 0.5°, show somewhat less distinct features.

Some of the shear zones have a minimum and a maximum radial velocity quite close to each other. This is consistent with the Doppler-signature of mesocyclones. However, strictly speaking one cannot be sure that cyclonic flow is indeed present. Comparing the velocity image of various elevations reveals that only the cyclonic flow associated with feature B has a vertical extent of more than 4 kilometers and persists for more than 15 minutes, which are prerequisites for qualifying it as a mesocyclone. Comparing the shear of radial velocity with the strength categories in use at the U.S. National Weather Service (fig.4.3) show that shear zone 1, however does not qualify as a mesocyclone, but falls in the “weak shear” category (using values of 9 m/s rotational velocity within a 2.0 km or 1.0 nm mesocyclone at 60 km or 33 nm from radar). The rotational velocity has been calculated by taking the difference between the maximum outbound and maximum inbound velocities divided by 2. A problem is that two data points near the center of the shear zone had no data. This is possibly due to filtering by the radar’s data processor. The data may have been automatically removed because the returned signal had a low normalized coherent power, which can be expected when the flow is very turbulent. It is possible that the shear zone would have met the criteria of a mesocyclone if the data were not removed.

The negative shear zones, 4 and 5, do not have regional radial velocity extrema. It is likely that these are not associated with meso(anti-)cyclones, but with downdrafts producing strong horizontal wind shear. The strongest 39 m/s wind gust was measured near or in shear zone 4.

The detection of potential mesocyclones embedded within this squall-line is quite remarkable. It suggests that the environments in which mesocyclones can develop may include situations of very low latent instability. In this case, mesocyclones have formed in conditions where not more than a few hundreds of J/kg CAPE were present.

It could be interesting to see how large the storm-relative helicity (SRH) is that the squall-line experienced, since it might be that high storm-relative helicity is conducive to the formation of mesocyclones within squall-lines just

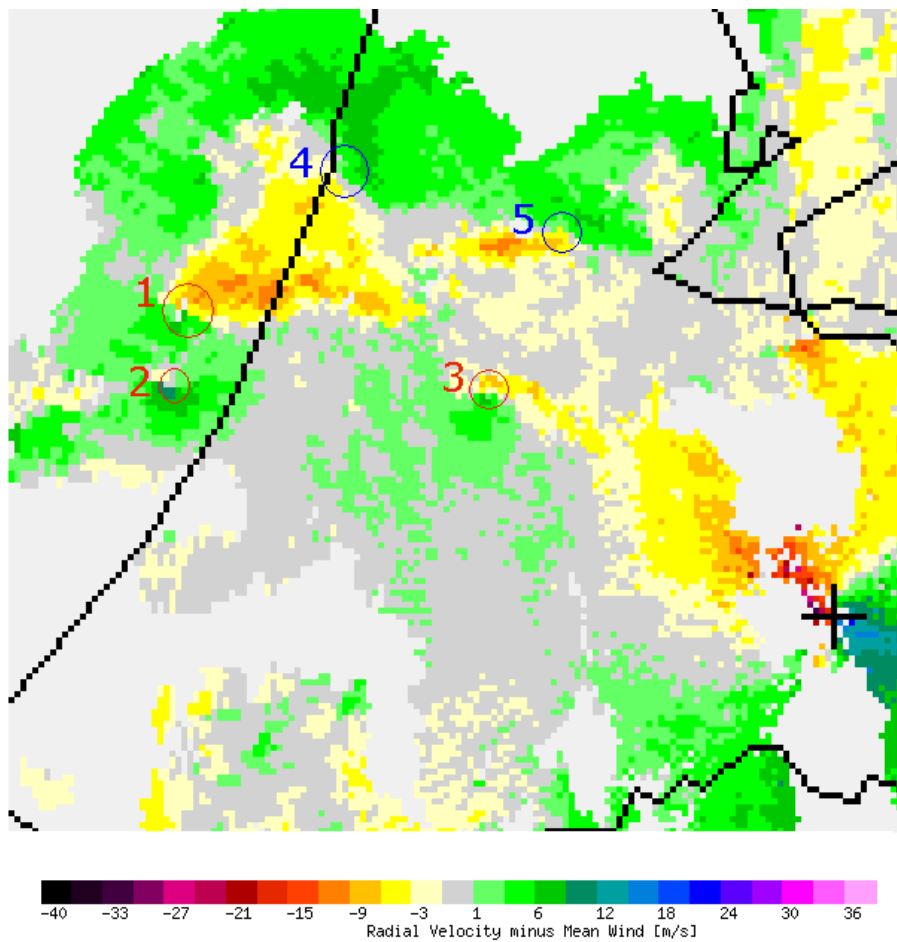


Figure 5.9: Filtered doppler velocities from a 2.0° elevation scan at 1509 UTC, January 28th 2003. Shown are the velocities minus a mean wind of 22 m/s from 270° . Positive numbers correspond with with a velocity component toward the radar and negative number with a component away from the radar. The radar site itself (De Bilt) is marked with a black cross.

as it is for supercellular mesocyclones. To do this, it is important to recognize that the helicity of the flow into the convective system should be calculated in a reference frame fixed with respect to the storm. It is customary to calculate the helicity with respect to a storm motion that is calculated beforehand. Here we can however exactly calculate the storm motion vector, since the storm motion vector can be deduced from the radar. For feature B we obtain a motion vector of 279° at 21.5 m/s. The corresponding 0-1 km SRH is 81 m^2/s^2 , and 0-3 km SRH is 77 m^2/s^2 .

It is hard to draw a conclusion from these values, because existing research has mainly focused on SRH in the environment of supercells. However, the values of 81 m^2/s^2 and 77 , can be said to be low in comparison with environments in which many supercell mesocyclones form¹. Also, it is remarkable that all helicity is present below an altitude of 1 km AGL. Different values of helicity are obtained by using the ID-method to estimate the storm-motion vector. Resulting in 305° at 22.7 m/s, this method yields SRH values of 258 m^2/s^2 and 243 m^2/s^2 respectively, which shows that one should not use the ID-method in this and similar cases to determine the storm motion.

Vertical cross-section

fig.5.10 shows cross-sections along the 150° radial at 1639 UTC, after the squall line has passed the radar site. It reveals quite clearly the squall-line flow pattern described by many authors. We see that low-level winds have a component toward the squall-line ahead of it. Behind the squall-line, the winds blow from rear to front at mid levels, the rear inflow jet, and from front to rear at high levels. The boundary between the two is also the boundary of the cold pool.

At the place of the highest echo tops there is radial convergence at low levels and divergence at higher levels. This can be explained by the presence of a strong updraft. The radial convergence zone extends over the cold pool backward up to mid-altitudes.

Behind the main convective line we see the front-to-rear-flow above the rear inflow jet. In contrast to the classical picture of a squall-line, we observe a large area of reflectivity ahead of the squall-line. This can be explained by the fact that upper-level winds were particularly strong, which has likely caused some of the precipitation to be transported downshear ahead of the squall-line. This resulted in moderate precipitation falling ahead of the main convective updraft zone.

The zone of even higher reflectivity at low-levels ahead of the squall-line is probably in part due to the formation of a bright band (see for example Doviak and Zrnić, 1993). A bright band is a quasi-horizontal band near level of zero wet bulb temperature. It is caused by melting snowflakes. Snowflakes are less effective scatterers than rain, but this is normally compensated for by their larger size. However, during the melting process, wet snowflakes are scatterers having the efficiency of rain and the size of snowflakes. This means their reflectivity is enhanced. Since in fig.5.10 the reflectivity has been linearly interpolated between the various reflectivity levels, we see that high reflectivities are only measured at the lowest elevation. This is around 500 m altitude, which

¹Supercell mesocyclones may form in environments of very low helicity as well through non-linear pressure perturbation effects. Theory predicts this to occur only in environments having substantial CAPE, which is not the case here.

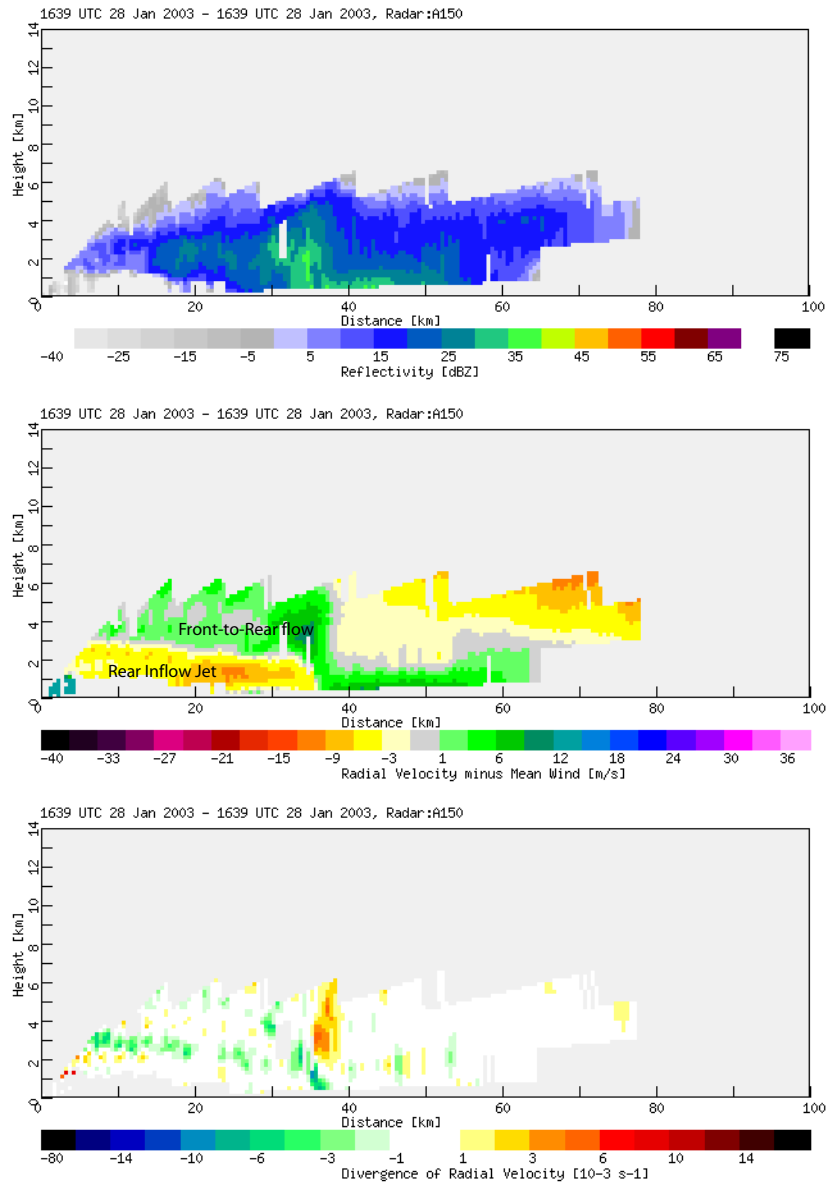


Figure 5.10: Vertical cross-section at 1639 UTC at an azimuth of 150° (black lines in fig.5.11). The images show reflectivity, radial velocity, and radial divergence. The values shown are obtained from PPI-scans of different elevations and interpolated between the elevations. The distance to the radar is plotted along the axes.

is near the height of the wet-bulb zero level according to the De Bilt sounding, so that we can indeed attribute the high reflectivities to a bright band. Behind the squall-line the wet bulb-zero level descends (almost) to the ground, so that possible bright banding occurs below the lowest radar elevation and is therefore not visible.

Line echo wave pattern and book-end vortex

As the squall-line moves inland, it gets a wavy pattern in the southwest, over Zeeland. The squall-line consists of several bow-shaped segments. It somewhat resembles a line echo wave pattern with waves having a relatively short wavelength compared with the LEWP's described in literature. These bow segments are associated with regions of enhanced rear to front flow and so that one can expect strong wind gusts to occur there (see e.g. Wakimoto, 2001).

At 1639 UTC the squall-line has moved inland. The multiple bows over the southwest have merged into one large bow, with a book-end vortex at its northern end. This vortex has a circulation that is much larger than a mesocyclone. It is quite strong having a shear of radial velocity of 24 m/s. There were no reports of severe weather associated with this vortex.

5.1.4 Case discussion

An important question is why the convection developed into a squall-line on that day. The most likely answer is that the upper trough provided lift in a linear-shaped area. Within this area, latent instability was generated by lifting and subsequent cooling of the mid-levels. The relatively stable layer around 800 hPa was removed by these processes and deep convection could initiate. Then a cold pool formed due to evaporation of rain into the sub-saturated air that was blowing into the trough from behind. The convection developed a more distinct linear organisation along the leading edge of the cold pool, where a zone of low-level convergence was present.

We observed bow-echo-like structures within a squall-line that may have caused higher gusts than those forecast by traditional methods. The small vortices that were observed may have led to high wind gusts as well. The strength of the features, exhibiting wind shears of 20 m/s over distances between 500 and 1000 m, are strong enough to be potentially hazardous to aviation especially during takeoffs and descents. Numerical simulations of convective systems, like those by Weisman and Davis (1998), see fig.3.5, develop vortices and bow-echo like features in high-shear environments only. So forecasters should probably be most alert for the development of such features in meteorological environments exhibiting high wind shear. Doppler-velocity data as well as reflectivity imagery of high resolution can be helpful in detecting them.

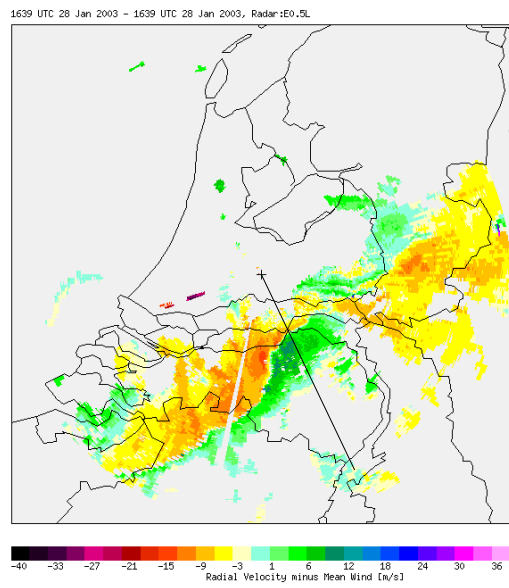
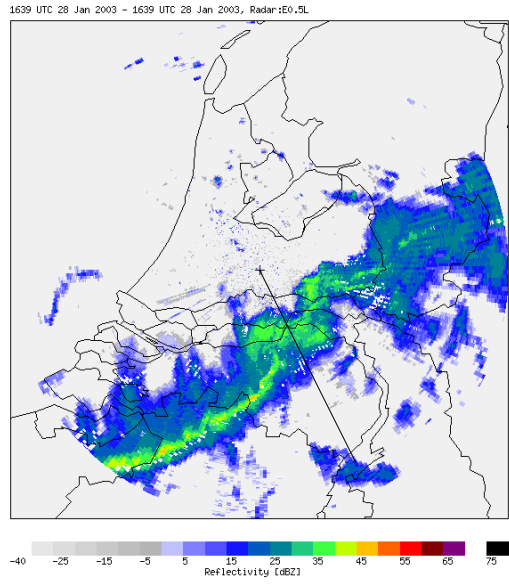


Figure 5.11: 0.5° PPI-scan at 1639 UTC, showing reflectivity (dBZ) and radial velocity (m/s) minus an average flow velocity (270 deg at 24 m/s). The black line denotes the cross-section shown in fig.5.9.

5.2 30th of July 2002, Multicell thunderstorms with strong outflows

5.2.1 Event description

During the afternoon of the 30th of July 2002 thunderstorms formed at various places over the Netherlands and Western Germany in an almost stagnant unstable air-mass. The thermodynamic environment was favorable for the development of strong outflows. The outflows from the storms over Germany merged to form one large cold pool that expanded westward. The leading outflow boundary, or gust front, accelerated westward over The Netherlands triggering new thunderstorm cells.

5.2.2 Synopsis

The synoptic environment of this event was characterized by low wind speeds throughout the troposphere and small horizontal temperature gradients (see fig.5.12). At 12 UTC, the 500 hPa analysis shows an area of high pressure located over Scandinavia and a trough from southern Ireland to southwestern France. Over The Netherlands, a weak south to southeasterly flow was present at the 500 hPa level.

At the surface, a weak thermal low was present over eastern France and southwestern Germany, see fig.5.13.

Instability and wind shear

There was quite some latent instability present as can be seen from the 12 UTC sounding from Valkenburg (06210) (fig.5.14). CAPE was about 1000 J/kg. The boundary layer is deep, well mixed and relatively dry. This allows for strong evaporation of precipitation with any storm that forms. The cooling of air that results can enable strong downdrafts to form, which was indeed what happened. The wind speed was quite low at all levels, so the wind speed of the downdrafts should be mostly attributed to evaporational cooling and internal storm dynamics and not to downward transport of horizontal momentum present at higher levels.

5.2.3 Radar data

The outflows of isolated storms occurring during the afternoon can be seen on the low-elevation radar scans. They are visible as lines of weak reflectivity, typically 0 - 7 dBZ. When such a line passes an observing station, the temperature drops and the surface wind direction changes and gets a component in the same direction as the outflow propagates. The clearest isolated outflow is that of a storm located near Amsterdam, whose outflow boundary can be seen to expand over much of Zuid-Holland.

A particular zone of low reflectivities can be seen to be located parallel to the coastline, about 10 km inland. It seems likely that this zone is associated with the sea-breeze front, given that surface winds have a wind component from the sea to the west of this line and a component from the land to the east of the line, leading to mass convergence at the surface.

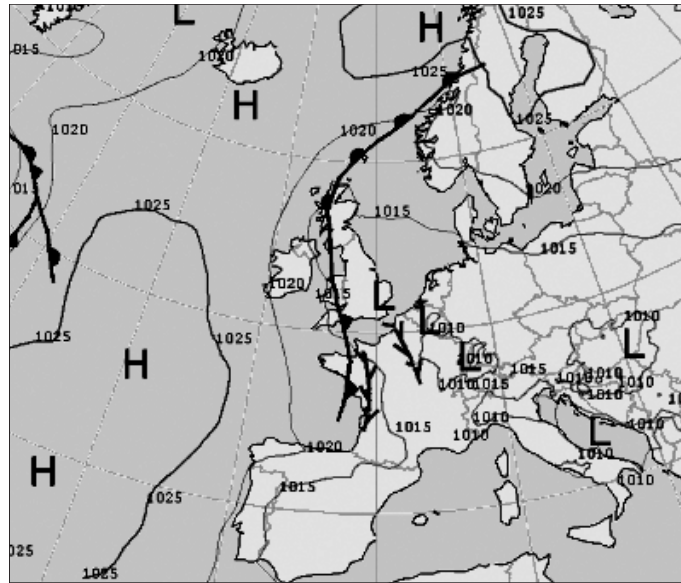


Figure 5.13: Surface analysis at 30 July 2002 12 UTC. Source: KNMI.

The reflectivity of outflow boundaries and convergence lines in general arises because mass convergence at the surface induces rising motions. Scatterers such as insects, dust and other aerosols are transported upward reaching the height where the 0.5 elevation scan can detect them. Another effect that may play a role is partial reflection of the radar beam caused by the different refractive indices of the air-masses on each side of the boundary (Doviak and Zrnić, 1993).

At the two latest pictures shown in fig.5.2.3, we can see the clustered system approaching from the east. The precipitation is preceded by a boundary that marks the leading edge of cold storm outflow. From the observations it can be seen where this boundary has passed, gusty easterly winds are reported and a temperature drop from near 30°C to around 20°C. A mesoscale analysis shown in fig.5.2.3 reveals that the cold air is associated with a mesoscale high pressure area. We find a surface pressure pattern that is quite similar to the pressure pattern of a gravity current (see fig.3.4). Ahead of the outflow boundary, slight pressure falls are observed over the west of The Netherlands, consistent with the development of a pre-squall mesoscale low pressure area.

The outflow boundary or gust front is clearly visible on a vertical cross-section. fig.5.17 shows the reflectivity, radial velocity and radial divergence in a vertical plane eastward at 1653 UTC. In this picture we see enhanced reflectivity at low altitudes at the leading edge of the outflow (at approximately 17 km distance from the radar). As can be expected, we detect velocities toward the radar behind this feature leading to strong convergence of radial velocity at the front itself.

Within the thunderstorm, there are two precipitation cores. Also, the trailing anvil that extends far eastward is clearly visible. The velocity image is particularly interesting. We can distinguish a rear-to-front flow located at about 3 to 4 km altitude on the back side of the system and descends to the ground at

06210 EHVB Valkenburg

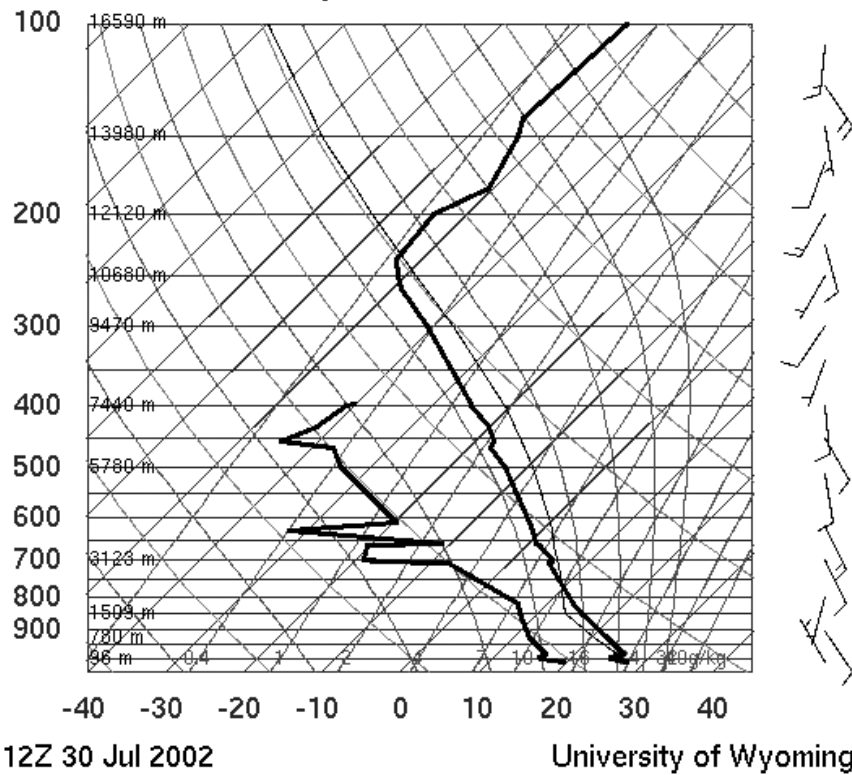


Figure 5.14: Skew-T log-p thermodynamic diagram showing sounding of 12 UTC, July 30th 2002 at Valkenburg. CAPE based on a parcel originating from a 50 hPa layer above the surface is 1000 J/kg. Source: University of Wyoming.

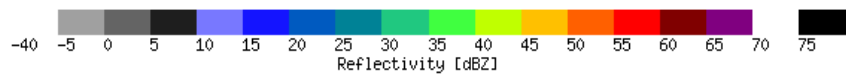
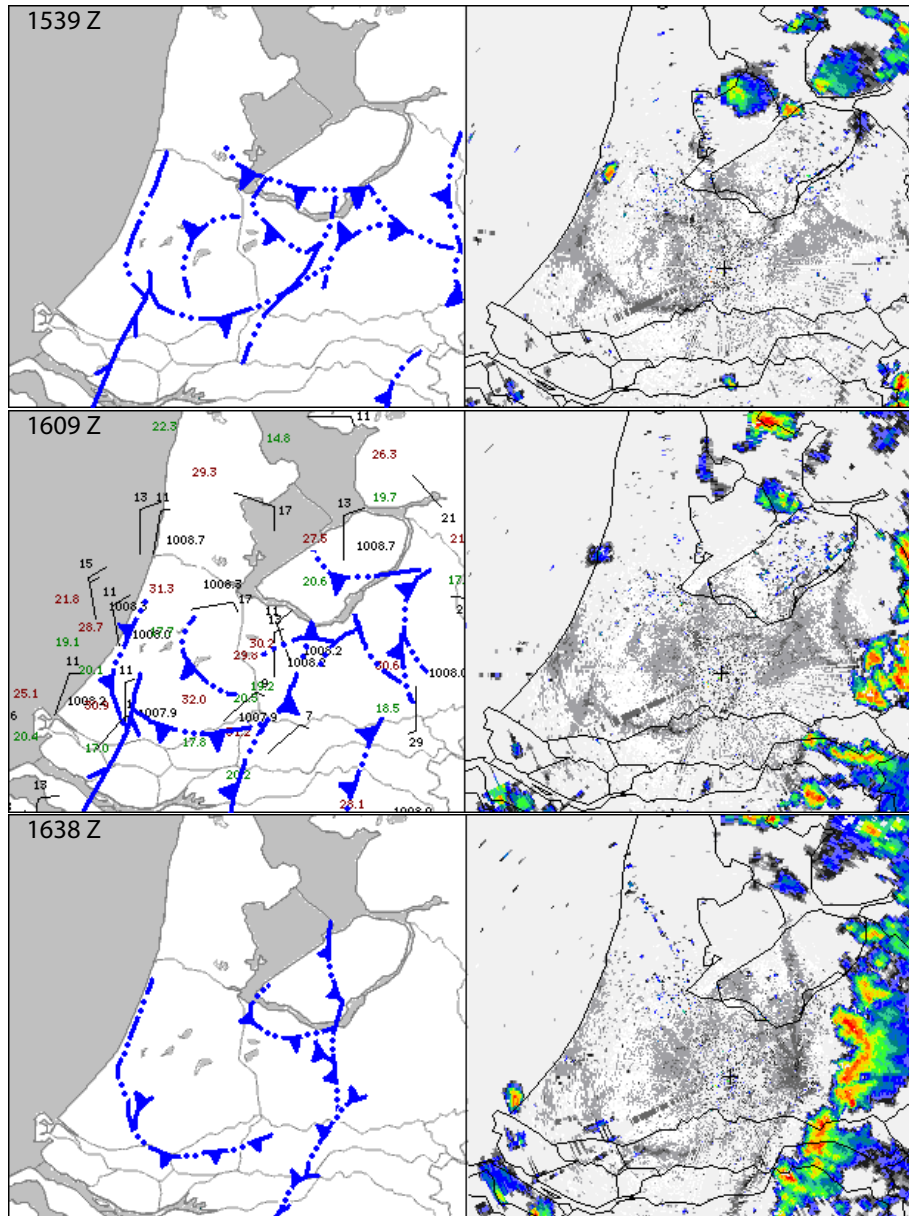
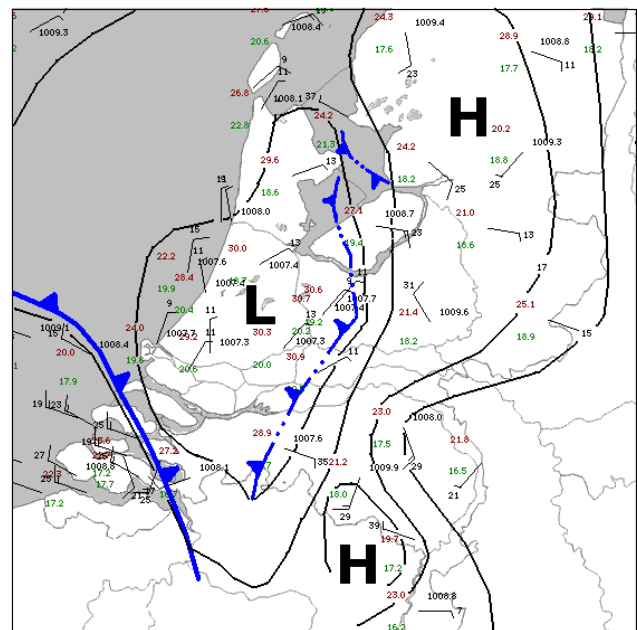
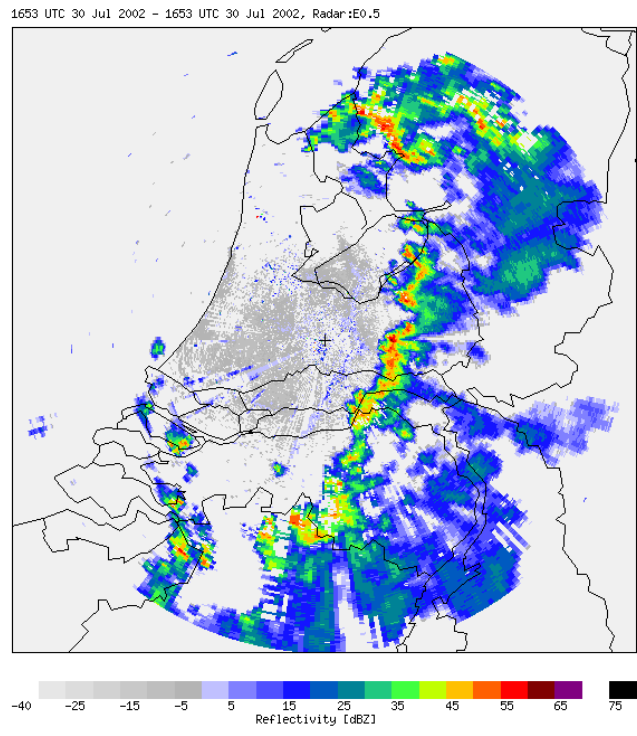


Figure 5.16: Reflectivity from a 0.5° elevation PPI scan from De Bilt at 1653 UTC and mesoscale analysis at 17 UTC. Black lines are isobars spaced 1 hPa. Line with triangles denotes a cold front. The blue line with triangles marks a cold front and the blue dotted line with triangles marks convective outflow boundaries.



its leading edge. This rear-to-front flow is can be described as descending rear inflow jet (RIJ). At the back side of the system a front-to-rear flow is present both above and under the RIJ. The front-to-rear flow below the RIJ originates from the area of radial divergence below the most intense precipitation core.

We can construct a two dimensional picture of the flow within the system, that is consistent with the distributions of radial velocity, radial divergence and reflectivity, which is shown in (fig.5.18). The two areas where high reflectivity is located above lower reflectivity are expected to be associated with updrafts in which precipitation particles form while being transported upward. The observed distribution of radial convergence below radial divergence is consistent with that. The precipitation that forms in each updraft is transported to the east by the front-to-rear flow where it leaves the updraft and falls down. It looks that the two updrafts are in different stages of their life cycles. The one closest to the gust front is the youngest. According to the theory of Lin et al. (1998)², this cell has been triggered when the gust front moved away far enough from former cell, that the compensating downdrafts did not the counteract the rising motions at the gust front. Indeed, it can be seen by inspecting a sequence of reflectivity images that the squall-line propagates westward in discrete steps, where new cells keep forming ahead of the older ones. A forecaster at the KNMI observed this discrete propagation, repeatedly seeing new cumuliform clouds develop ahead of older updrafts as the storms approached from the east (Huiskamp, pers. comm.).

5.2.4 Case discussion

The passage of the gust front caused severe wind gusts, strong enough to cause trees to be uprooted. Uprooted trees were reported in Allingawier (north of The Netherlands), Utrecht (center), Udenhout and Berkel-Enschot (south) (VWK, 2002). Apart from this isolated wind damage, there was also one report of large hail from the town of Zwiggelte, were hailstones having a diameter of 3 cm were observed.

The potential of strong gusts could be anticipated, given that a very deep sub-saturated cloud layer was observed by the radiosonde measurements and there was ample CAPE to sustain deep thunderstorms. The large coverage of storms further enhanced the potential of severe gusts, because it led to the formation of one large cold pool. The gravity current along the cold pool boundary or gust front can then add to the gusts caused by downdrafts of the individual convective cells. At the KNMI the forecasters found the estimation of the storm coverage to be the most difficult aspect of the forecast (van der Haven, pers. comm.). If the coverage of storms had been smaller, the cold pool would have been weaker and the potential for damaging wind gusts would have been much smaller.

²see also section 3.2

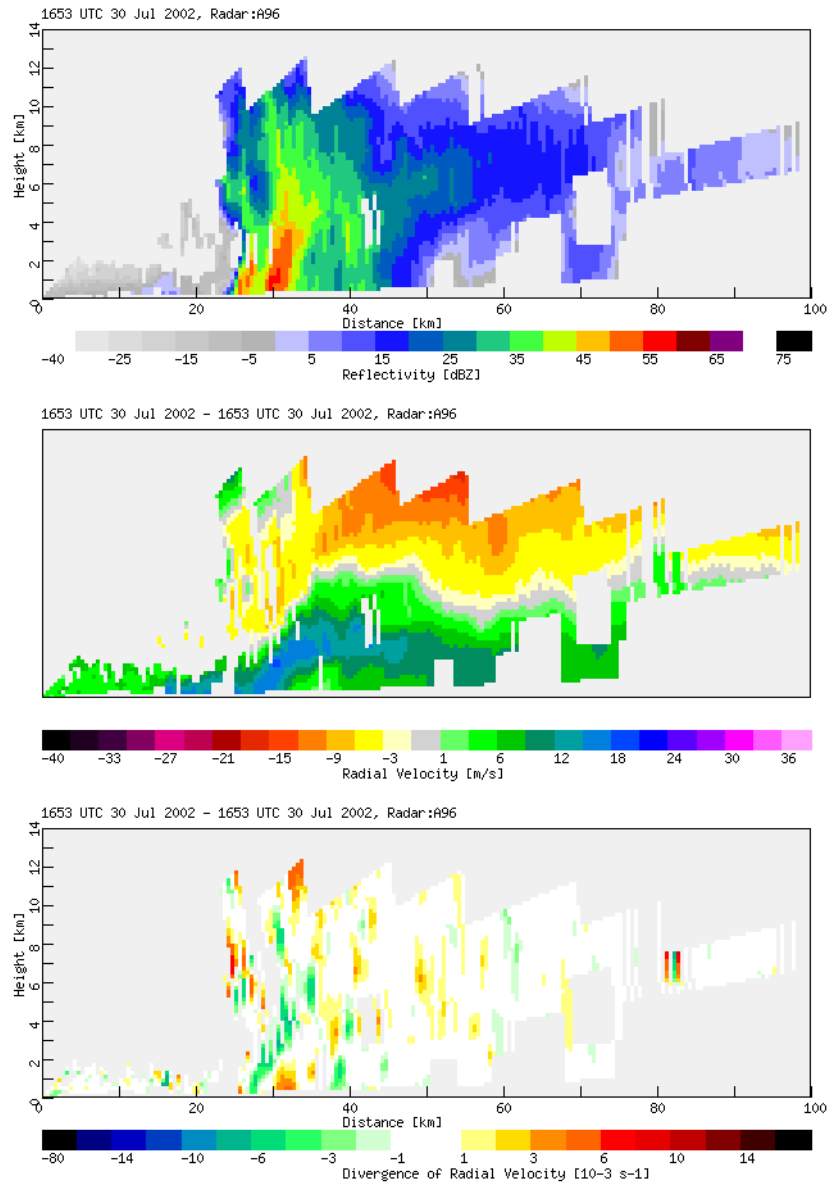


Figure 5.17: Vertical cross-section at an azimuth of 96° from De Bilt at 1653 UTC July 30 2002. The images show reflectivity (dBZ), radial velocity (m/s) and radial divergence (10^{-3} s^{-1}) respectively.

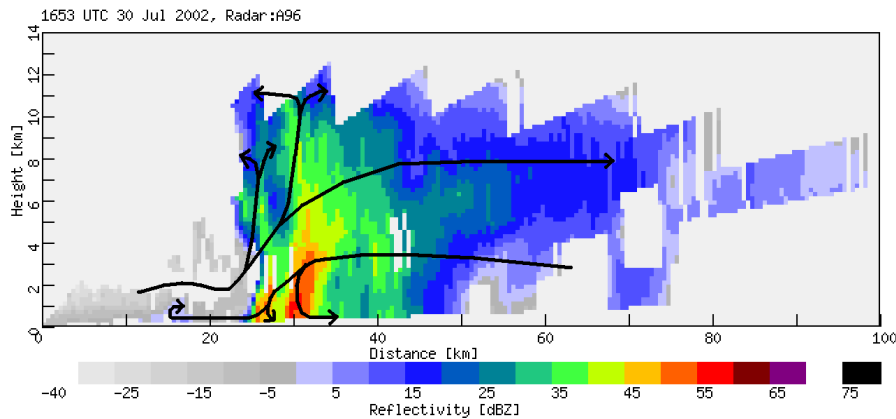


Figure 5.18: Cross-section showing a deduced two-dimensional flow pattern in a storm-relative reference frame.

5.3 Embedded HP-mini-supercell, 2nd of May 2003

5.3.1 Event description

In the afternoon 2nd of May 2003, several lines of linear convection passed The Netherlands from the southwest to northeast. Within one of these lines that developed over the southwestern Netherlands, a low-topped supercell developed, that had HP-supercell characteristics. It produced wind damage and localized large hail over the western half of The Netherlands.

5.3.2 Synopsis

Instability

An intense upper-level trough was approaching The Netherlands from the southwest as a moderately warm air-mass was present over the area, that had steep low-level lapse rates (see fig.5.23), but no significant latent instability. On the analysis maps of the 300 hPa and 500 hPa level, a mid/upper-jet streak can be identified from the eastern Bay of Biscay to the Channel region. During the afternoon the left part of its exit region moved over The Netherlands leading to upward vertical motion in the area. The upward motions (and possibly also cold air advection) lead to a significant cooling of the mid-troposphere between 12 UTC and 00 UTC as can be seen from the soundings taken at De Bilt at 12 UTC and 00 UTC (fig.5.23). The temperature at the 500 hPa level dropped from -23°C at 12 UTC to -28°C at 00 UTC. In the mean time, at lower levels, there was also cooling taking place: at 850 hPa temperatures dropped from 6°C to 1°C in the same period. However, because the moisture content of the air at low-levels increased – surface dew-point temperatures rose from 9°C to 13°C in De Bilt between 12 UTC and 17 UTC – latent instability likely developed. The NCEP GFS 12 UTC model run produced a lowest-30hPa CAPE of 250 -

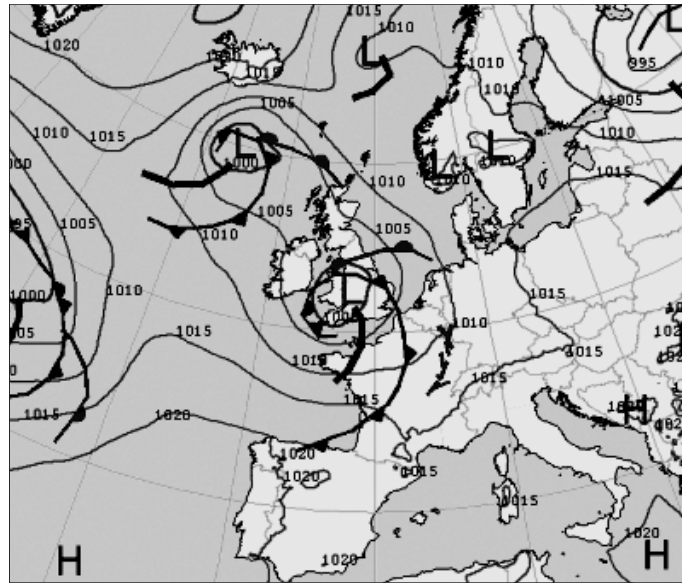


Figure 5.19: Surface analysis at 2 May 2003 12 UTC. Source: KNMI.

500 J/kg over The Netherlands at 18 UTC. The HiRLAM model initialized at 12 UTC forecast surface based-CAPE near 500 J/kg at 18 UTC.

5.3.3 Radar data

Fig.5.25 shows the reflectivity from a 0.5° elevation scan from De Bilt at 1654 UTC in addition to surface observations and a (subjective) pressure analysis. We see the linear system that formed over the southwest of The Netherlands, which moves northeastward. In agreement with RKW-theory the strong low-level shear has caused the gust front (the location of which can be inferred from the radial velocity data) not to have propagated far ahead of the leading convective line.

Just south of a zone of very high reflectivity a notch can be seen in the leading line of the system. The radial velocity shows strong azimuthal shear of radial velocity having two extrema close to each other near the location of this notch. These are the characteristic signatures of two mesocyclones. fig.5.26 shows the evolution of this part of the convective system by combining fragments of the reflectivity and velocity data at six different times in one picture. At 1623 UTC, a signature of cyclonic convergence is located on the eastern flank of an area of high reflectivity west of Rotterdam. Cyclonic convergence is seen in a radial velocity image as a mixture of a signature of cyclonic flow (i.e. azimuthal shear of radial velocity) and convergent flow (i.e. radial shear of radial velocity). In the next time steps this feature becomes relatively more cyclonic and less convergent as it moves northeastward. At 1638 UTC, the signature can be seen to consist of two centers of circulation. The velocity data from scans at higher elevations (not shown) learn that these two centers can also be distinguished at higher altitudes. In the centers of the circulations some data is missing. The data

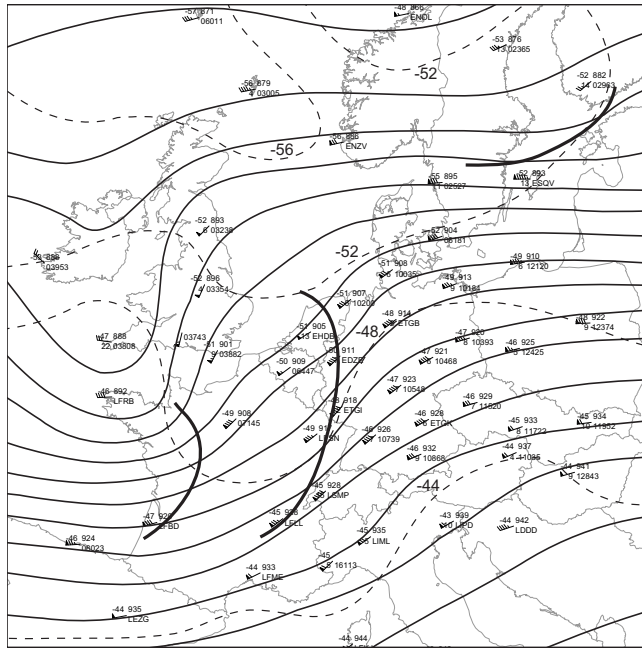


Figure 5.20: Observation plots and analysis by the author of the 300 hPa surface on 2 May 2003 at 12 UTC. The solid lines are geopotential height contours drawn every 5 gdam. The dashed lines are isotherms drawn every 4 °C. Thick line is a shortwave trough. Station plots consist of a conventional wind-vane, temperature (in °C, top left), dew point depression (in °C, bottom left), geopotential height (in gdam, top right) and WMO or ICAO identifier (bottom right).

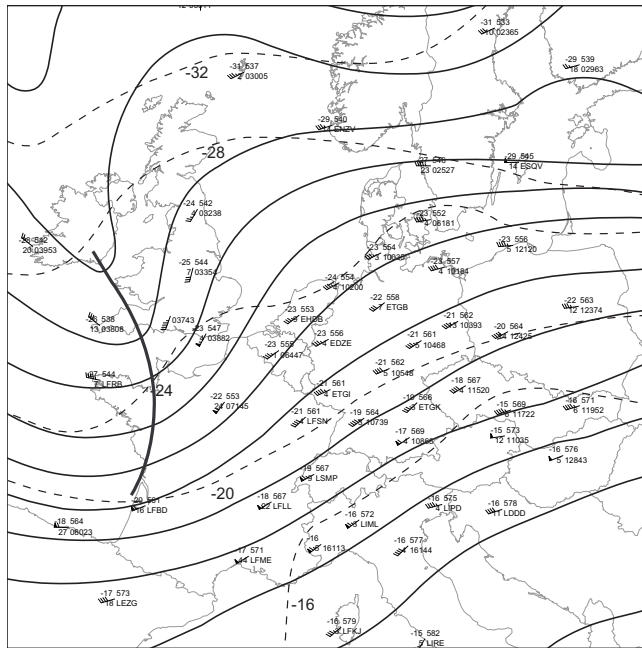


Figure 5.21: Observation plots and analysis by the author of the 500 hPa surface.

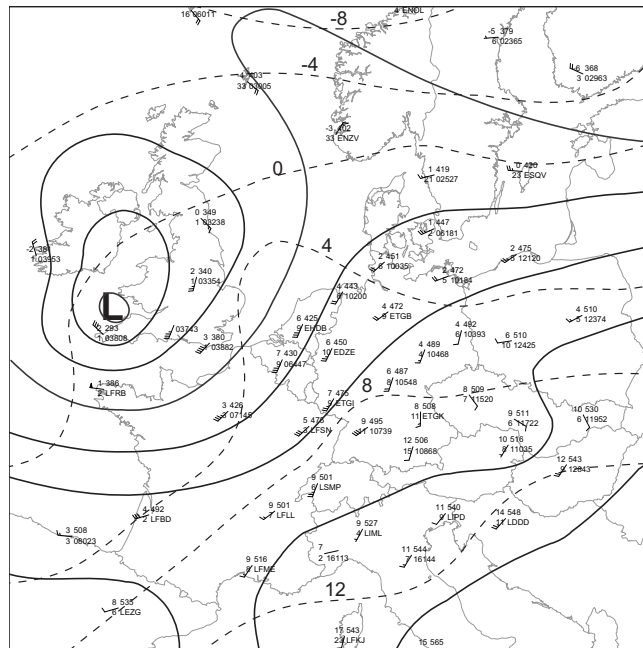


Figure 5.22: Observation plots and analysis by the author of the 850 hPa surface.

at those points have likely been removed by the radar’s internal processor that filters on normalized coherent power (as was also the case on the data of 28 January), so that the exact strength of the circulations cannot be detected.

The two centers can be seen to move slightly apart from each other over time and are intensifying. As far as the remaining data allows for an estimation of the strength of the circulation, it seems that the most westerly circulation reaches its peak intensity in the 0.5° elevation scan at 1654 UTC. It has a rotational velocity of 15 m/s at that time at a distance of approximately 25 nm from the radar, which puts it in the “moderate mesocyclone” category (see fig.4.3). The eastern circulation has its peak intensity in the 1708 UTC scan, reaching a rotational velocity of 18 m/s, which also qualifies it as a “moderate mesocyclone”. At this time, the circulation has its maximum inbound and outbound velocities in two adjacent pixels leading to 36 m/s shear over approximately 500 m.. This kind of radial velocity signature is known as a *tornado vortex signature* (TVS). In contrast to what its name seems to imply, TVS’s are not always associated with tornadoes. So, from this radar data only we cannot tell that a tornado occurred at that place at that time.

Severe weather

The path of the eastern circulation coincides with the towns of Amstelveen and Diemen, where between 70 and 80 reports of wind damage were reported to the local fire department just after the storm passed (Fire Service website, 2003). The fire service attributed the damage, which consisted of tens of cars being crushed by falling trees and minor damage to buildings, to a tornado (Dutch:

06260 EHDB De Bilt

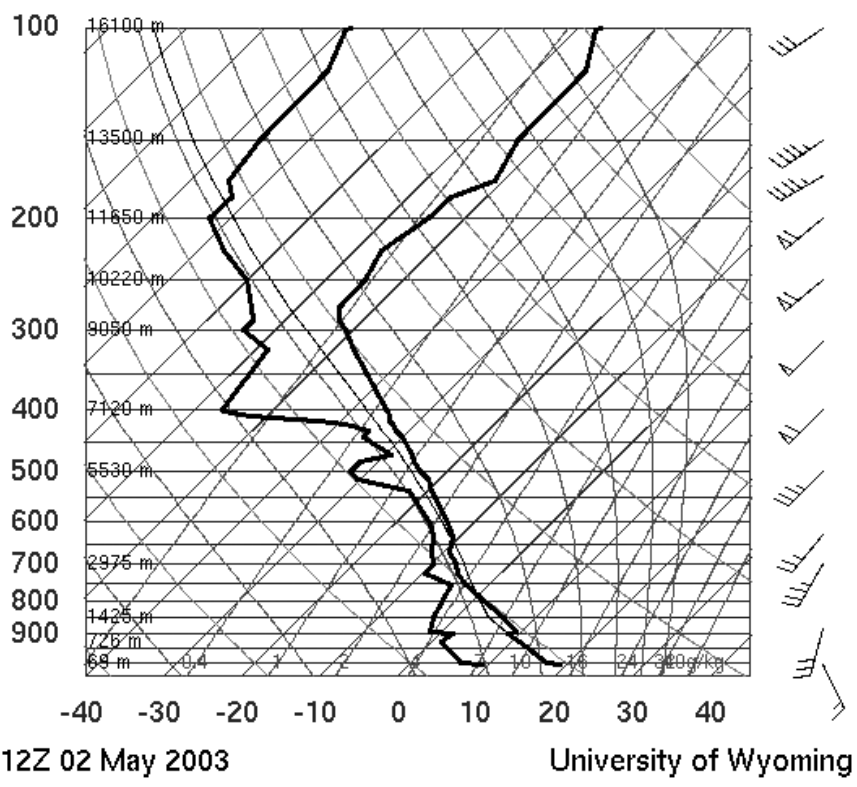


Figure 5.23: Skew-T log-p thermodynamic diagram showing sounding of 12 UTC, May 2nd 2003 at De Bilt. Source: University of Wyoming.

06260 EHDB De Bilt

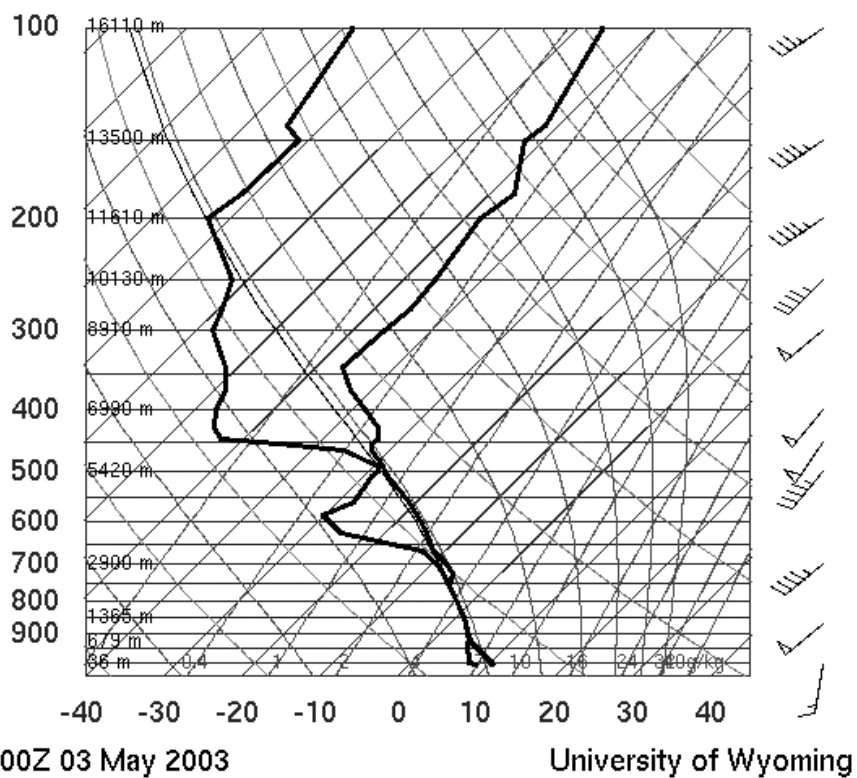


Figure 5.24: Skew-T log-p thermodynamic diagram showing sounding of 00 UTC, May 3rd 2003 at De Bilt. Source: University of Wyoming.

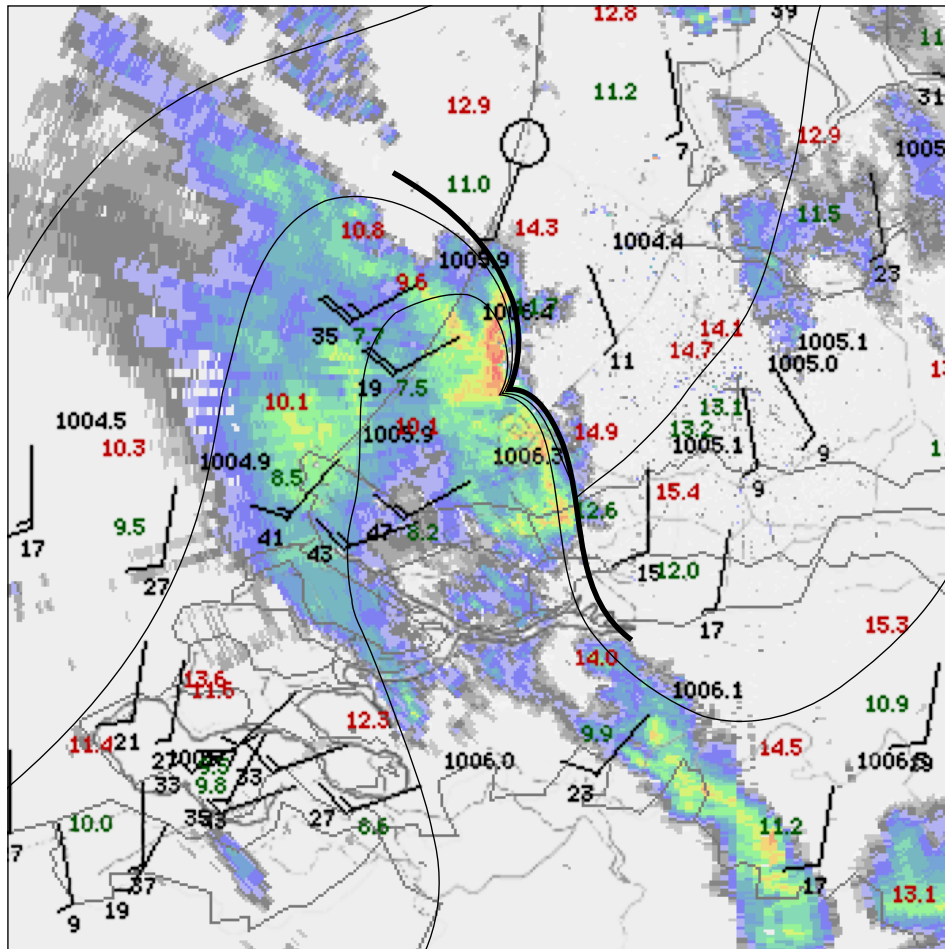


Figure 5.25: 0.5° elevation reflectivity from De Bilt at 1654 UTC, synoptic observations at 1700 UTC and (subjective) pressure analysis. The thick line corresponds with the gust front of the convective system.

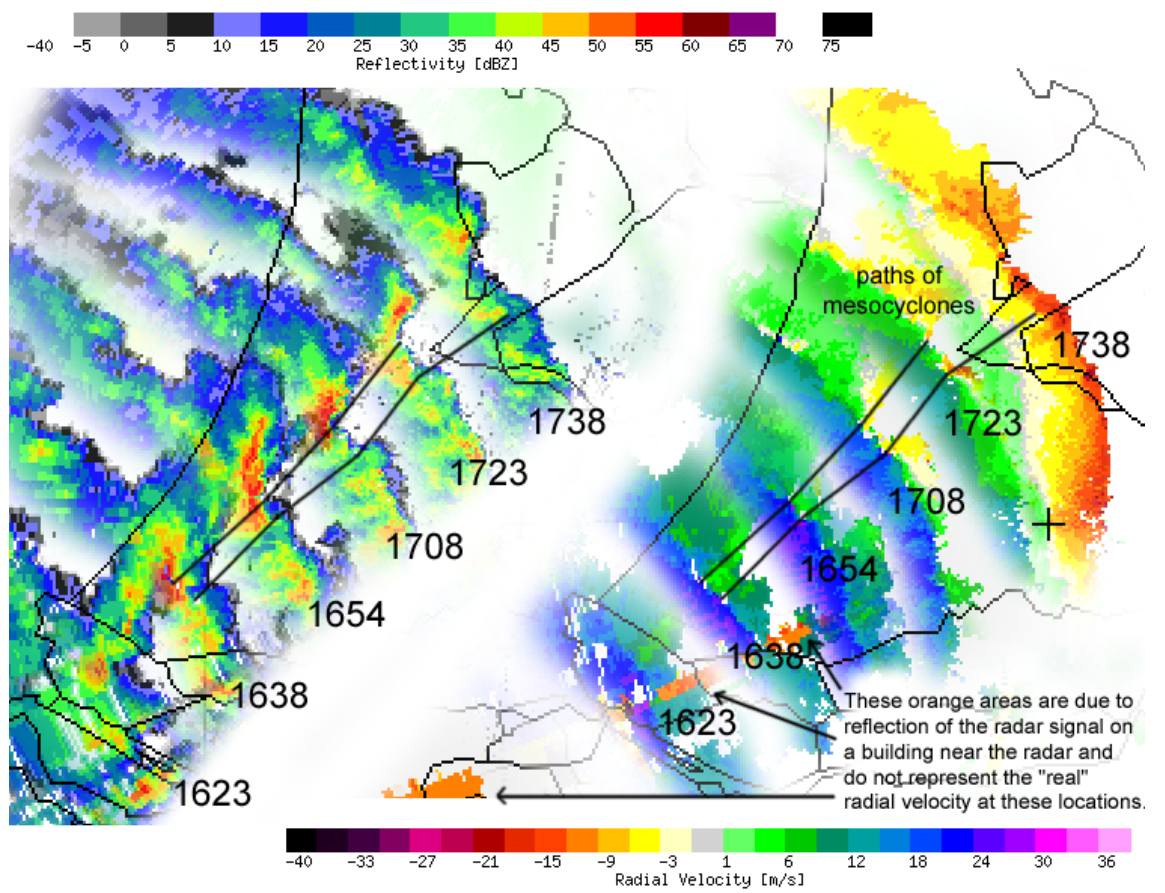


Figure 5.26: Fragments of 0.5° scans from De Bilt. Shown are reflectivity (left, in dBZ) and radial velocity (right, in m/s). Black lines denote the paths of two mesocyclonic circulations

“windhoos”). In the hour before this happened, minor damage to buildings and uprooted trees was reported along the storm’s path as well. Quite severe damage was done near the town of Noorden where 6000 m² of greenhouses were demolished. The complete press release by press association (ANP) is given in the Appendix. At synoptic stations, the highest gusts associated with this convective line were 23 m/s at Rotterdam airport, 23 m/s at Schiphol airport and 24 m/s on the pier in IJmuiden. This illustrates the point that even quite dense meteorological observation networks are not likely to detect the most severe gusts that happen with thunderstorms.

The origin of mesocyclonic rotation

In the entire troposphere, wind speeds increased on approach of the upper trough. During the first half of the afternoon, winds veered from south-southeast to southwesterly direction with height, consistent with quasi-geostrophic warm advection. Gradually, low-level winds veered to southwesterly directions as well with exception of the lowest parts of the boundary layer. Quite strong shear developed within the boundary layer as surface winds remained southerly to south-southeasterly at about 5 m/s, while 850 hPa winds increased to 18 m/s from the southwest. Especially ahead of the linear convective system in which the supercell developed, surface winds were somewhat backed with respect to the wind at the top of the boundary layer. However, this has not resulted in high values of helicity.

A hodograph is constructed that is thought to be more or less representative of the flow ahead of the storm. We have used the surface wind at 17 UTC at Schiphol airport (approximately 15 minutes before the cell was over the airport), the Doppler-derived wind profile at De Bilt (below 2 kilometer altitude) and the wind profile of the HiRLAM model at 18 UTC above that altitude (fig.5.27). This hodograph is associated with only 15 m²/s² 0-1 km storm-relative helicity, where the storm motion vector is 221° at 20 m/s. 0-3 km storm relative helicity was -11 m²/s². Normally, one would expect values on the order of a few hundreds m²/s².

It is a possibility that ingestion of baroclinically induced vorticity has played an important role in sustaining the observed mesocyclone. In addition to the storm hodograph, fig.5.27 shows the (non-density weighted) average 0-1 km wind (215° at 10 m/s) and a vector representing the storm-relative 0-1 km wind (45° at 10 m/s). From the radar reflectivity imagery it can be seen that these northeasterly storm-relative low-level winds approach the mesocyclone just to the east of an area of strong reflectivity, where the air is likely to be cooled by evaporation of precipitation. One would expect that there is a temperature gradient approximately perpendicular to the storm-relative low-level winds at low levels. This can have caused generation of vorticity with an axis parallel to the storm-relative inflow (i.e. streamwise vorticity) which upon tilting into the updraft produces cyclonic vorticity.

Cross-section

A cross-section from De Bilt through the eastern mesocyclone at 1708 UTC is shown in fig.5.28. The mesocyclone was at that time located at 30 km from the radar. A bounded weak-echo region, be it not very clear, can be seen to extend

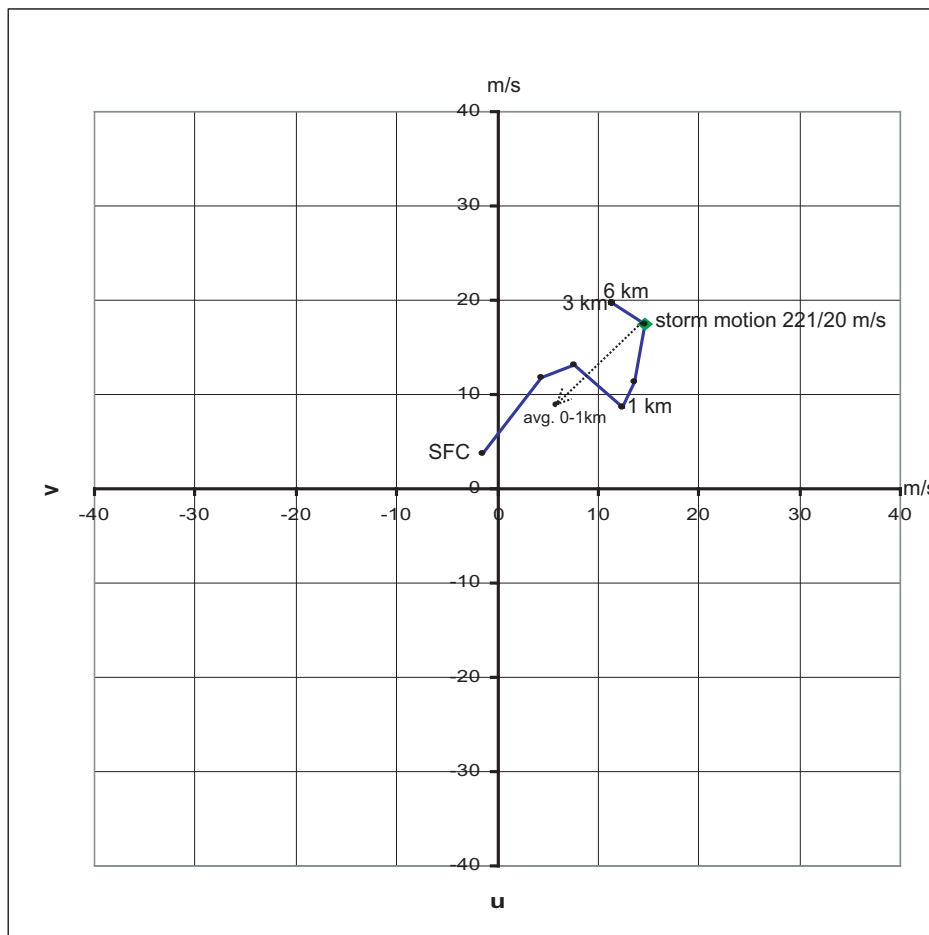


Figure 5.27: Hodograph constructed from the surface wind at 17 UTC at Schiphol airport (approximately 15 minutes before the cell was located over the airport), the Doppler-derived wind profile at De Bilt (below 2 kilometer altitude) and the wind profile of the HiRLAM model at 18 UTC above that altitude. The diamond denotes the radar-derived storm motion. The dotted arrow points to the 0-1 km average wind (210° at 10 m/s) and represents the storm-relative 0-1 km wind (45° at 10 m/s).

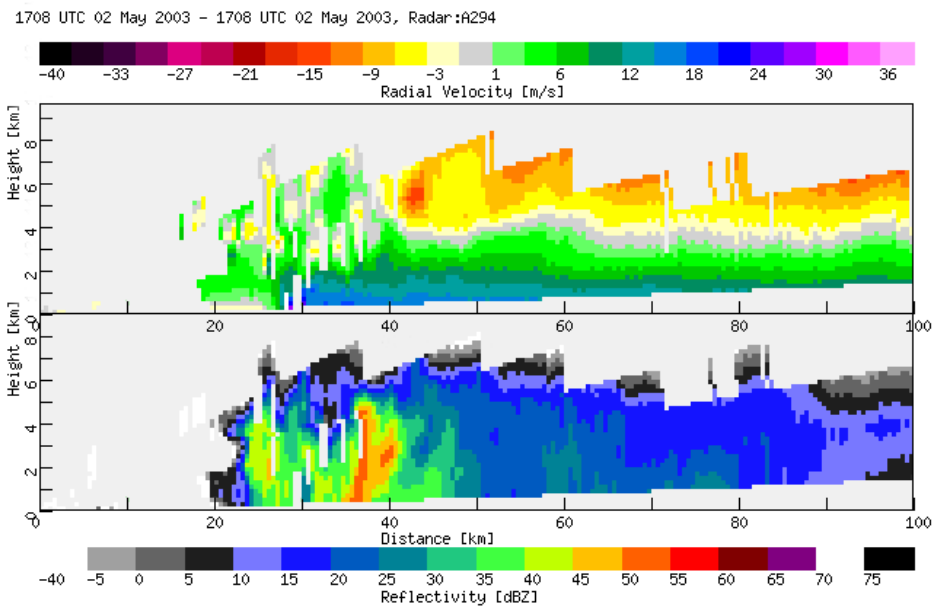


Figure 5.28: Cross-section through the eastern mesocyclone at 1708 UTC.

upward from the surface to approximately 1.5 kilometers. The reflectivity at low levels is between 25 and 30 dBZ where it is in the 40-45 dBZ range higher aloft. Such a signature is indicative of a strong updraft (see section on supercell morphology). Other cross-sections that were investigated did not show clearer (bounded) weak echo regions either. At 35 km distance, the strong downdraft to the northwest of the westernmost updraft can be seen, which is associated with a core of high reflectivity extending upward to approximately 5.5 km. The whole storm complex has low tops of around 6 to 7 km. This characteristic in combination with its relatively small horizontal size, makes that this supercell falls in the mini-supercell category. Since it also has HP-characteristics and is embedded within a squall-line, it can best be described as an *embedded HP mini-supercell*.

Chapter 6

Conclusions and recommendations

6.1 Radar

“Raw” Doppler radar data has proved to be quite useful in studying severe deep moist convection. More information can be extracted than what is contained in the radar products that are currently in use at the KNMI. These products include a the standard reflectivity product that combines reflectivity data from the De Bilt radar and a radar in Den Helder to form one image. Two other products, a hail detection product (Holleman et al., 2000; Holleman, 2001) and an echo-top-height (ETH) product are currently operational. The standard reflectivity product projects the raw data on a 2 x 2 kilometer grid and assigns different colors to 6 different reflectivity intervals. The lowest reflectivity interval starts at 7 dBZ and the highest starts at 47 dBZ and includes all values higher than that.

The findings in this report suggest that the following additions or modifications to the products could be useful:

- increasing the resolution of the reflectivity product, which allows for identification of small-scale structures in the reflectivity field (for example to 1x1 km).
- adding the possibility to distinguish lower and higher levels of reflectivity, which can be useful for detecting outflow boundaries (low reflectivity) and detecting structures within storm cores (high-reflectivity).
- the use of radial velocity data in general and the development of products for detecting e.g. mesocyclones, wind shear zones and downbursts in particular.

The second recommendation is incorporated in a new version of the reflectivity product that is being developed at the KNMI. This product does not use fixed reflectivity-intervals but gives the end-user the exact reflectivity value. The end-user can then present the data in the way he prefers, including or excluding low or high levels of reflectivity.

In contrast to the possibilities the radar yields, it should be noted that the data presented herein still contain a number of errors that have to be dealt with when using it as a basis for products based on this data. Firstly, there are artifacts of the Dual-PRF technique visible in both the reflectivity and the velocity image. Reflectivity and velocity tend to fluctuate up and down a bit every ray. Secondly, velocity unfolding is not error-free. Even the filtering algorithm by Holleman and Beekhuis (2003) leaves some errors in the data. This is particularly a problem when one wants to develop automatic detection algorithms for mesocyclones, shear zones and downbursts. One would encounter a lot of false alarms if the error cannot be removed from the data before applying the detection algorithms. Finally, the radar processor that is currently in use, automatically filters out data points that have a low normalized coherent power, which in practice means that data points are often filtered out in the centers of mesocyclones, which reduces the probability of detecting them.

Not only do these errors and processing artifacts make the development of new products more difficult, they also require the user to have a high skill in interpreting the data. Within the KNMI it might be useful to make the raw data presented herein available to forecasters because of the added value it has over the current reflectivity product. The product could also be useful for other parties having the skill to interpret the data correctly. For most other users it would be preferred that the existing errors in the data be resolved first. It also seems that velocity data, which is particularly hard to interpret, could perhaps best be combined with detection algorithms for shear zones, mesocyclones and downbursts. These can enable the meteorologist, who is under large pressure at the time of a severe convective event, to discover such features quickly. Additionally, a cell-tracking algorithm could be developed, which may be helpful to anticipate which areas are to be affected by the storm. In fact, dr. Holleman (KNMI/WM/WA) is planning to work on this starting in the second half of 2003.

For the developing such algorithms, it might be useful to modify the volume scanning scheme slightly. The radar now scans at elevations of 0.5° , 2.0° , 3.5° and seven higher elevations. At a moderate to large distance from the radar, like for example 120 km, scanning at 2.0° elevation means scanning at 4.0 km above the earth's surface (neglecting the earth's curvature and density effects). An algorithm detecting a shallow reflectivity or velocity feature would then be relying on the 0.5° elevation scan data only. Therefore it may be wise to change the scheme to include a 1.0° elevation scan.

6.2 Convective forecasting

Having studied three different cases, a few conclusions can be drawn that apply to severe deep moist convection in The Netherlands in general.

The cases herein occurred in environments of low latent instability as compared with most cases described in literature. In the strong shear cases (January and May cases) it was too low to be detected by the operational radiosonde network. This seems however to be consistent with the find made by many authors that for severe storms strong shear may compensate for low CAPE. This implies that, in contrast to what one could infer from low values of CAPE obtained with parcel theory, severe convection may very well occur in a Dutch winter as well

as in summertime.

Strong shear allows for storms to develop their own internal dynamics, which indeed was observed. On January 28th 2003 the squall-line contained embedded vortices and bow echoes. On May 2nd 2003 an embedded low-topped HPish supercell was detected containing two moderately strong mesocyclones. Surface observations and media reports on storm damage seem to suggest that in both cases severe weather was concentrated near these features. This suggests that forecasters should give attention to the development or movement of such features whenever they can be detected or can be forecast.

6.2.1 Recommendations for enhancement severe (convective) storm forecasting at the KNMI

There seem to be two different paths to go to enhance the KNMI's ability to warn the public for dangerous convective weather events. One path is enhancing the *nowcasting* capabilities of the operational forecasters. This can be done by providing more tools that can make detection of features (i.e. mesocyclones, downbursts, gust fronts) that may produce severe weather more easy, as was described above. But, on the other hand, forecasters should be trained to handle these tools and check them for correctness. They should know basic physical theory about the features as well in order to be able to translate the observations into a diagnosis and a short-term forecast.

The other path focuses on the *forecasting* capabilities, that can be enhanced if meteorological settings that may produce severe storms can be recognized better and earlier. In order to be able to do this, forecasters should study both theory and practice. A lot of theory is available in scientific literature, but is poorly accessible and not specifically written with the "forecaster" in mind. A systematic way to make this knowledge applicable in operational practice is the development of *conceptual models*. These conceptual models could for example describe

- the hazards that may be expected,
- the meteorological setting (quantity and quality of instability/wind shear/forcing), i.e. the forecasting aspect,
- the physical mechanism behind the convective structure,
- how the phenomenon can be detected/recognized using radar, satellite and other sensors,
- and a number of case-studies.

This list may be augmented with convective indices that are thought to be typical for the respective convective phenomenon. However, one should realize that parameters should be verified before they are put into use. It is important to realize what a particular parameter exactly forecasts. A parameter that is a good predictor of thunderstorm occurrence may in fact be a poor predictor of *severe* thunderstorm occurrence. Another consideration is that some parameters have been verified with statistical methods, but are hard to interpret from a physical point of view. "Using methods having minimal physical bases means it will be difficult to predict when a method will fail because the understanding

of how it works is not available.” (Doswell, 2001). Therefore severe storm forecasting is likely to be most successful if, in addition to tools having statistical bases, physical understanding of severe storms is present as well.

Appendix: Press release on severe weather occurring on May 2nd 2003

Schade door noodweer

2 mei 2003

DEN HAAG (ANP) - Zware onweersbuien hebben vrijdagavond flinke schade aangericht in Zuid-Holland. Met name de lijn Boskoop, Bodegraven, Alphen aan den Rijn, Noorden en Leimuiden werd volgens de brandweer zwaar getroffen. In het plaatsje Noorden werd 6000 vierkante meter kassen vernield. Omgevallen bomen en een blikseminslag hinderden het treinverkeer.

Op de Zoetermeer Stadslijn tussen Den Haag en Zoetermeer reden vrijdagavond door omgewaaide bomen een paar uur minder treinen. Op de Hofpleinlijn lag om dezelfde reden het treinverkeer enige tijd stil tot aan Leidschendam-Voorburg. Door blikseminslag reden er enige tijd minder treinen tussen Haarlem en Leiden.

In Boskoop waaide een gevel uit een woning. Verder vielen er bomen op auto's en waaide een aantal auto's tegen elkaar aan. Het heftige noodweer legde ook een schuur tegen de vlakte. Daarbij kwam asbest vrij. De brandweer neemt daar de nodige maatregelen om te voorkomen dat het asbest zich verspreidt.

In Den Haag liepen rioleringen over, waardoor sommige woningen met wateroverlast te kampen kregen. In het Westland werd een woning getroffen door een omgewaaide boom. In Den Haag viel een boom op een auto, deelde de Haagse brandweer mee.

Een windhoos heeft vrijdagavond in Amstelveen en Diemen veel schade veroorzaakt. De brandweer van de regio Amsterdam kreeg in twee uur tijd zeventig tot tachtig meldingen van schade aan huizen en gebouwen en omgewaaide bomen. Persoonlijke ongelukken hebben zich niet voorgedaan.

Volgens de brandweer zijn tientallen auto's door bomen geplet en kregen bewoners te maken met waterschade door weggewaaid dakdelen. Ook schoorstenen begaven het. De windhoos vond plaats aan het begin van de avond en duurde slechts een paar minuten.

References

- Bluestein, H.B. and C.R. Parks, 1983: A synoptic and photographic climatology of low-precipitation severe thunderstorms in the southern plains. *Mon. Wea. Rev.*, **111**, 2034–2046.
- Browning, K. A., 1964: Airflow and precipitation trajectories within severe storms that travel to the right of the winds. *J. Atmos. Sci.*, **21**, 634–639.
- Bunkers, M. J., B. A. Klimowski, J. W. Zeitler, R. L. Thompson, and M. L. Weisman, 2000: Predicting supercell motion using a new hodograph technique. *Wea. Forecasting*, **15**, 61–79.
- Burgess, D.W., R.R. Lee, S.S. Parker, and D.L. Floyd, 1995: A study of mini supercell thunderstorms. Preprints, *27th Conf. on Radar Meteor.*, Vail, Colorado, Amer. Meteor. Soc. 4–6.
- , and L. R. Lemon, 1991: Characteristics of mesocyclones detected during a NEXRAD test. Preprints, *25th Int'l Conference on Radar Meteorology*, Norman, Oklahoma, American Meteorological Society, 39–42.
- , R.R. Lee, S.S. Parker, D.L. Floyd and D.L. Andra, 1995: A Study of Mini Supercells observed by WSR-88D radars, Preprints, *27th Conf. on Radar Meteorology*, Vail, CO, Amer. Meteor. Soc., 4–6.
- Craven, J. P., H. E. Brooks, and J. A. Hart, 2002: Baseline climatology of sounding derived parameters associated with deep, moist convection. Preprints, *21st Conference on Severe Local Storms*, San Antonio, Texas, American Meteorological Society, 643–646.
- Chisholm A. J. and J. H. Renick, 1972: The kinematics of multicell and supercell Alberta hailstorms, *Alberta Hail Studies*, 1972, Research Council of Alberta Hail Studies Rep. 72-2, 24–31.
- Davies-Jones, R., 1984: Streamwise vorticity: The Origin of Updraft Rotation in Supercell Storms, *J. Atmos. Sci.*, **41**, 2991–3006.
- Dessens, J. and J.T. Snow, 1989: Tornadoes in France. *Wea. Forecasting*, **4**, 110–132.
- Doswell, C. A., III, 2001: Severe Convective Storms: An Overview, in: *Severe Convective Storms*, Meteorological Monograph Vol.28, #50, Amer. Met. Soc., Boston., 1–26.
- , III and Burgess, D.W., 1993: Tornadoes and tornadic storms: A review of conceptual models. *The tornado: Its Structure, Dynamics, Prediction, and Hazards*, Geophys. Monogr., No.79, Amer. Geophys. Union, 557–571.

- _____, III and E.N. Rasmussen, 1994: The effect of neglecting the virtual temperature correction on CAPE calculations. *Wea. Forecasting*, **9**, 619-623.
- _____, III and P.M. Markowski, 2001: Is buoyancy a relative quantity?, submitted as a note to *J. Atmos. Sci.*
- Dotzek, N., 2001: Tornadoes in Germany, *Atmos. Res.*, **56**, 233-251.
- _____, 2002: Text available at http://www.essl.org/pdf/ESSL_PilotStudy.pdf.
- _____, 2003: An updated estimate of tornado occurrence in Europe, submitted to *Atmos. Res.*. Text available at <http://www.op.dlr.de/~pa4p/pdf/ecss02s.pdf>.
- Doviak, R. J. and D.S. Zrnić, 1993: *Doppler radar and Weather Observations*, 2nd ed., Academic Press, San Diego – London, 562 pp.
- Emanuel, K.A., 1994: *Atmospheric Convection*, Oxford University Press, New York, 580 pp.
- Fire Service website: <http://www.brandweer.nl>.
- Fovell, R. and Ogura Y., 1988: Numerical Simulation of a Midlatitude Squall Line in Two Dimensions, *J. Atmos. Sci.*, **45**, 3846-3879.
- Gatzen, G. P., 2003: A Derecho in Europe: Berlin, 10 July 2002, submitted to *Wea. Forecasting*.
- Grant, B. N., and R. Prentice, 1996: Mesocyclone Characteristics of Mini Supercell Thunderstorms. Preprints, *15th Conf. on Weather Analysis and Forecasting*, Norfolk, VA., American Meteorological Society, 362-365.
- Groenland, R., 2002: De boog-echo van 7 juni 1997, *Meteorologica*, 10 nr. 4.
- Hanstrum, B. N., Mills, G.A., Watson, A., Monteverdi, J.P., and Doswell, C.A.III, 2002: The cool season tornadoes of California and Australia, *Wea. Forecasting*, **17**, 705-722.
- Holleman, I., H.R.A. Wessels, J.R.A. Onvlee, and S.J.M. Barlag, 2000: Development of a Hail-Detection-Product, *Phys. Chem. Earth B*, **25**, 1293-1297.
- Holleman, I., 2001: Hail detection using single-polarization radar, Scientific report, KNMI WR-2001-01.
- Holleman, I., 2002: Wind Profiling by Doppler Weather Radar, COST-720 Workshop on “Integrated Ground-Based Remote Sensing Stations for Atmospheric Profiling”, L’Aquila, Italy.
- Holleman, I., and Beekhuis H., 2003: Analysis and Correction of Dual-PRF Velocity Data, *J. Atmos. Ocean. Technol.*, **20**, 443-453.
- Holzer, A.M., 2001: Tornado climatology of Austria, *Atmospheric Research*, **56**, 203-211.
- Houze, R. A. Jr., 1993: *Cloud Dynamics*, Academic Press, 570 pp.
- Johnson, R.H. and P.J. Hamilton, 1988: The relationship of surface pressure features to the precipitation and air flow structures of an intense midlatitude squall-lines., *Mon. Wea. Rev.*, **116**, 1444-1472.
- Kroll, E., K. Floor, H. Geurts, R. Mureau, T. Opsteegh and P. Siegmund, 1995: *De wereld van het weer*, Stichting educatieve omroep Teleac, Utrecht, 188 pp.
- Kuiper, J. and M. De Hond, 1999: De zware hagelbuien van 6 juni 1998, *Meteorologica*, **8** nr. 1.

- LeMone, M. A., 1983: Momentum Transport by a Line of Cumulonimbus, *J. Atmos. Sci.*, **40**, 1815–1834.
- Lin, Y.H., R.L. Deal and M.S. Kulie, 1998: Mechanisms of Cell Regeneration, Development, and Propagation within a Two-Dimensional Multicell Storm, *J. Atmos. Sci.*, **55**, 1867–1886.
- Moller, A.R., C.A. Doswell, III, and R.W. Przybylinski, 1990: High-Precipitation Supercells: A Conceptual Model and Documentation. Preprints, *16th Conf. Severe Local Storms*, Kananaskis Park, Alberta, Canada, AMS (Boston), 52–57.
- Moller, A.R., 2001: Severe Local Storms Forecasting, in: *Severe Convective Storms*, Meteorological Monograph Vol.28, #50, Am. Met. Soc., Boston., 433–480.
- Monteverdi, J.P. and J. Quadros, 1994: Convective and rotational Parameters Associated with Three Tornado Episodes in Northern and Central California, *Wea. Forecasting*, **9**, 285–300.
- , C.A. Doswell and G.S. Lipari, 2000: Shear Parameter Thresholds for Forecasting tornadic Thunderstorms in northern and central California, Preprints, *20th AMS Conf. on Severe Local Storms*, Orlando, Florida.
- Rasmussen, E.N., 2002: Refined Supercell and Tornado Forecast Parameters, accepted in *Wea. Forecasting*, text available at <http://www.nssl.noaa.gov/~erik/www/SSR/index.htm>.
- Rasmussen and Blanchard, 1998: A Baseline climatology of Sounding-Derived Supercell and Tornado Forecast parameters, *Wea. Forecasting*, **13**, 1148–1164.
- Rasmussen, E. N., and J. M. Straka, 1998: Variations in supercell morphology. Part I: Observations of the role of upper-level storm-relative flow. *Mon. Wea. Rev.*, **126**, 2406–2421.
- Rinehart, R.E., 2001: *Radar for Meteorologists*, 3rd print, Rinehart publications, Columbia MO, 428 pp.
- Rotunno, R. and J.B. Klemp, 1982: The Influence of the Shear-Induced Pressure Gradient on Thunderstorm Motion, *Mon. Wea. Rev.*, **110**, 136–151.
- Rotunno, R., J.B. Klemp and M.L. Weisman, 1988: A theory for Long-Lived Squall-Lines, *J. Atmos. Sci.*, **45**, 463–485.
- RMI, 2000: *Klimatologisch overzicht 1999* (Dutch/French), Royal Meteorological Institute (Belgium), Uccle.
- Schmocker, G.K., R.W. Przybylinski, and Y.J. Lin, 1996: Forecasting the initial onset of damaging downburst winds associated with a mesoscale convective system (MCS) using the mid-altitude radial convergence (MARC) signature. Preprints, *15th Conf. on Weather Analysis and Forecasting*, Norfolk, VA., Amer. Meteor. Soc., 306–311.
- Schultz, D.M., P.N. Schumacher, and C. A. Doswell III, 2000: The intricacies of instabilities, *Mon. Wea. Rev.*, **128**, 4143–4148.
- VWK, 2002: “Onweer”, *Weerspiegel*, **9**, The Dutch Climatological and Meteorological organisation VWK, 885–890.
- Weisman, M.L., J.B. Klemp and R. Rotunno, 1988: Structure and Evolution of Numerically Simulated Squall Lines, *J. Atmos. Sci.*, **45**, 1990–2013.

- Weisman, M.L. and C.A. Davis, 1998: Mechanisms for the Generation of Mesoscale Vortices within Quasi-Linear Convective Systems, *J. Atmos. Sci.*, **55**, 2603–2622.
- Weisman, M.L., 2001: Bow echoes: A tribute to T. T. Fujita, *Bull. Am. Meteor. Soc.*, **82**, 97–116.
- Wessels, H.R.A., 1968: De zware windhozen van 25 juni 1967, *Hemel en Dampkring*, **66**, 155–178.
- Wicker, L.J., and L. Cantrell, 1996. The role of vertical buoyancy distributions in miniature supercells. Preprints, *18th Severe Local Storms Conf.*, San Francisco, CA, Amer. Meteor. Soc., 225–229.